ELSEVIER

Biophysical Chemistry 67 (1997) 1–25

Biophysical Chemistry

Evaluation of intrinsic chemical kinetics and transient product spectra from time-resolved spectroscopic data

Andrei K. Dioumaev *

Department of Physiology and Biophysics, University of California, Irvine, CA 92697, USA

Received 15 July 1996; revised 17 December 1996; accepted 17 December 1996

Abstract

This communication is devoted to the evaluation of true spectra and intrinsic (microscopic) rate constants from apparent kinetics measured in time-resolved spectroscopic experiments monitoring complex relaxation dynamics of multi-intermediate systems. Retinal proteins, cytochrom *c* oxidase, phytochrome, hemoglobin, and photoactive yellow protein are examples of natural systems in which several transient states (intermediates) overlap so strongly, both in time and spectral domains, that their isolation and full characterization by classical biochemical methods is impossible, and mathematical evaluation of their true spectra and microscopic kinetic constants is required. Most of the popular methods for analysis of kinetic data, global fitting (GF), singular value decomposition (SVD), principal component analysis (PCA) and factor analysis (FA), are applicable to two-dimensional (2D, in time and spectral domains) arrays of data. All these methods produce only a phenomenological description of data, that approximates the measured data only with apparent kinetics. A fundamental limitation, namely, insufficient information in 2D data, does not allow any of these methods to reach the final goal: to recalculate from apparent to intrinsic values in any but the most trivial cases. A strategy was proposed (J.F. Nagle, Biophys. J., 59 (1991) 476–487) to include an additional (third) information-rich dimension, temperature, into the simultaneous computer analysis. A simultaneous direct fitting of 3D data arrays to systems of differential rate equations allows recalculation of apparent kinetics into true spectra and intrinsic rate constants. In spite of its evident theoretical advantages, this strategy has not been successful on real data. Here we describe another custom-built program, *SCHEMEFIT*, developed for the same purpose: to fit measured kinetics directly to the system of coupled differential rate equations describing the photochrome's relaxation dynamics. Though sharing the main strategy with the previous approach, *SCHEMEFIT* is based on a different set of numeric algorithms, and its application requires different tactics. Its performance is illustrated on synthetic data, and compared with GF and SVD. An example of applying *SCHEMEFIT* to the photocycle of halorhodopsin is also reported. © 1997 Elsevier Science B.V.

Keywords: Global fitting; Singular value decomposition, SVD; Kinetic data analysis; Chemometrics; Intrinsic kinetics; Halorhodopsin

* Tel: (714)-824-7783; Fax: (714)-824-8540; E-mail: dioumaev@orion.oac.uci.edu

PII S0301-4622(96)02268-5

1. Glossary

$\Delta\mathbf{A}(\lambda,t)$	a 2D N_λ by N_t matrix of time-resolved spectroscopic data for a particular set of external conditions, e.g. temperature, pH, etc.
$\Delta\mathbf{A}_{\text{experiment}}(\lambda,t,T)$	a 3D N_λ by N_t by N_T matrix of time-resolved experimental data for a particular set of external conditions, e.g. pH, salts, etc.
$\Delta\mathbf{A}_{\text{theory}}(\lambda,t,T)$	a 3D N_λ by N_t by N_T matrix approximating experimental data array for a particular set of external conditions, e.g. pH, salts, etc.
Ac{**X**}	autocorrelation in vector **X**, see Eq. (17) and Eq. (18)
$\mathbf{B}(\lambda,j)$	an N_λ by N_e matrix of amplitudes of exponentials, obtained by GF
$\mathbf{C}(i,t)$	an (N_i+1) by N_t matrix of true concentrations of transient states
$\mathbf{C}(i,t,T)$	a corresponding 3D, (N_i+1) by N_t by N_T, matrix
$\mathbf{D}(i,j)$	an (N_i+1) by (N_i+1) matrix of eigen-vectors of the **M**-matrix
$\mathbf{E}(\lambda,i)$	an N_λ by N_i matrix of true differential extinctions of intermediates
$f(j,t)$	time-dependent functions in GF, e.g. exponentials for pseudo-first order reactions
FRAC(j)	fractional indicator function (see Eq. (20)) for estimating N_{SVD}
ΔG_{ij}	free energy difference between states i and j, $\Delta G = \Delta H - \Delta S \cdot T$
$\Delta G^{\#}(i,j)$	free energy barrier between states i and j, $\Delta G^{\#} = \Delta H^{\#} - \Delta S^{\#} \cdot T$
ΔH_{ij}	enthalpy difference between states i and j
$\Delta H^{\#}(i,j)$	enthalpy barrier between states i and j
h	Planck's constant
IND(j)	indicator function (see Eq. (21)) for estimating N_{SVD}
$\mathbf{K}(i,j)$	an (N_i+1) by (N_i+1) matrix of intrinsic rate constants defining the kinetic scheme of the transformations
K_{XY}	intrinsic rate constant defining the spontaneous reaction from state X to state Y
k	Boltzmann constant
$\mathbf{k}^*$	a vector of eigen-values of **M**-matrix, containing (N_i+1) elements
$\mathbf{k}_{\text{GT}}$	a vector of time constants, produced by GF, (N_e+1) elements
$\mathbf{M}(i,j)$	an (N_i+1) by (N_i+1) matrix of coefficients of coupled differential equations, describing the system under study
N_c	number of statistically valid exponentials in GF
N_i	number of transient states involved (besides the unexcited state)

N_{fit} a parameter in *SCHEMEFIT* determining the number of "unsuccessful" iterations, before a step-wise decrease in the search volume is to take place

N_{SVD} number of statistically valid components in SVD

N_t number of time points in time-resolved measurements

N_T number of temperatures at which the time-resolved measurements were performed for creating the 3D data array for scheme fitting

N_λ number of measured points in spectral domain

P an $(N_i + 1)$ by $(N_i + 1)$ matrix of coefficients defined by Eq. (15)

R an N_λ by $(N_i + 1)$ matrix of coefficients defined by Eq. (16)

RSMR root square mean of residuals between the measured and the fitted function

S an N_λ by N_λ (if $N_\lambda > N_t$) or N_t by N_t (if $N_\lambda < N_t$) diagonal matrix of singular values (i.e. square root of the eigen-values of matrix $\Delta\mathbf{A}(\lambda,t)$), produced by SVD

ΔS_{ij} entropy difference between states i and j

$\Delta S^{\#}(i,j)$ entropy barrier between states i and j

T absolute temperature

t time

U an N_λ by N_t matrix of basis spectra, produced by SVD

V an N_t by N_t matrix of apparent kinetics of the basis spectra, produced by SVD

α a coefficient in *SCHEMEFIT* for gradual adjustment of the search volume

β a coefficient in *SCHEMEFIT* for step-wise decrease in the search volume

γ a coefficient in *SCHEMEFIT* determining the number of times the step-wise decrease in the search volume is to take place

$\delta(\lambda,t,T)$ 3D matrix of noise in experimentally measured data

$\varphi(\mathrm{T})$ excitation efficiency (percentage of photo-transformation)

λ wavelength/wavenumber

σ_δ mean noise, i.e. a square root of noise dispersion

$\sigma_{\Delta G(i,j)}$ dispersion in values of $\Delta G^{\#}$ during minimization by the adaptive random search algorithm

$\sigma_{\Delta H(i,j)}$ dispersion in values of $\Delta H^{\#}$ during minimization by the adaptive random search algorithm

2. Introduction

Application of modern time-resolved instrumental methods to optical monitoring of chemical/biochemical reactions has made it possible to study the complex dynamics of natural photochromic systems. Relaxation dynamics of photo-induced reactions in bacteriorhodopsin [1–17], halorhodopsin [18–20], visual rhodopsin [21–23], cytochrome *c* oxidase [24,25], phytochrome [26], hemoglobin [27], and photoactive yellow protein (PYP, from *Ectothiorhodospira*) [28,29] have in each case revealed several metastable states (intermediates), coexisting on time scales from sub-picoseconds to sub-seconds. Full characterization of the photocycle intermediates and the pathways of their transformation is an essential step for evaluating the molecular mechanism of the functionings of these proteins. However, most of the intermediates cannot be stabilized and isolated in a pure form, and their accurate characterization cannot therefore be achieved by traditional biochemical methods. These intermediates are interconnected by a complex pattern of cross-transitions with temporal overlap resulting from pronounced back-reactions and/or branched pathways. Furthermore, the intermediates' spectra are usually broad, while the corresponding spectral shifts during the photocycle are relatively small, leading to spectral overlap. As a result, the measured transient absorbance change, at *any* wavelength/wavenumber and at *any* time point, *always* reflects a mixture of contributions from several intermediates.

This means that such transient states can be *isolated* only mathematically, and they can be fully studied only after deconvolution by a computer analysis. The limiting factor is the ability of mathematical algorithms to deconvolute the measured raw kinetic data into true intrinsic properties of the intermediates.

Analysis of time-resolved kinetic traces has previously been performed (in most cases) by one of two methods [1]: *global fitting* (GF) [30–32] and *singular value decomposition* (SVD) [33–36], or by some combination of these two [1,2,21,30,37,38]. One of the goals of this communication is to analyze the fundamental limitations of these methods. This is illustrated on arrays of synthetic data in Section 5. The focus of that section is to show that, despite widespread belief, not only GF but also SVD (and PCA, and FA) analyses provide only a *phenomenological* description of data, stopping short from evaluating the pure intermediates' spectra and intrinsic kinetics (i.e. microscopic rate constants). Mathematically, this is a trivial result (see below), since both GF and SVD are applied to two-dimensional data arrays (2D, in wavelength/wavenumber and time domains), which do not contain enough information for unambiguous deconvolution of the involved intrinsic kinetics and pure intermediates' spectra.

Both GF and SVD make full use of all the information available in the corresponding 2D data array. Therefore, further progress requires additional information. Nagle [8] proposed including a third dimension, temperature, in the *simultaneous* computer analysis. It was shown theoretically, and illustrated on synthetic data [8,9], that such 3D data arrays contain enough information to go one step further, as compared to the phenomenological description provided by 2D analysis either by GF or SVD methods. The 3D simultaneous analysis allows a derivation of the complete *kinetic scheme*, and extraction of intrinsic, rather than apparent, rate constants, as well as the pure intermediates' spectra. Unfortunately, this approach, as its author puts it [17], "has yet to be successful on real data". In spite of its evident advantages, it was used only in three publications on the bacteriorhodopsin photocycle [8,13,17].

Based on the approach of Nagle [8], a new software package *SCHEMEFIT* was custom-designed by the author of this communication. Using a more powerful set of numerical algorithms, the program directly fits 3D data arrays to differential rate equations describing complex patterns of intermediates' interconversions, including back reactions, transient equilibria, and branching. The ability and precision of the *SCHEMEFIT* package to perform this task is illustrated on synthetic data in Section 7.1. Section 7.2 describes application of *SCHEMEFIT* to the analysis of real data, the photocycle of halorhodopsin.

[1] Principal component analysis (PCA), the foundation of "factor analysis" (FA), might be listed as a third method. Since it produces the same result as SVD (though by somewhat different computational algorithm), we shall not discuss it here separately.

3. Materials and methods

The custom-built software package *SCHEMEFIT* was developed in the C programming language under the UNIX operational system. Eigensystem-solving procedures are from "netlib/eispack" of the public domain library of the AT & T Bell Labs (Murray Hill, NJ); their conversion from FORTRAN to C was done using the "f2c" package of the same origin. Most computations were done on a DEC Alpha AXP 3000/500 175 MHz workstation (Digital Equipment Corporation) under OSF/1. On this workstation, one iteration of *SCHEMEFIT* takes approx. 20 ms of CPU time, and takes an order of magnitude longer on an in Intel-based PC with 486DX50 processor. The portability of *SCHEMEFIT* was checked for the following platforms: ULTRIX, OSF/1, CONVEX/OS, IBM/AIX-3 (GNU C compiler); and, using a reduced version of *SCHEMEFIT* (due to memory limitations), for PC-DOS with the Borland C compiler.

Global fitting was performed with a program *FITEXP*, developed earlier in the General Physics Institute (Moscow, Russia) by Dr. N.V. Tkachenko, with contributions by V.I. Chukharev, A.Yu. Sharonov and A.K. Dioumaev [12,39]. SVD analysis was performed in MatLab (The Math Works, Inc., Sherborn, MA). A program for the F-test statistics was based on the algorithm from Ref. [40]. Data visualization and scientific drawing were done either in IDL (Research Systems, Inc. Boulder, CO), or in MatLab. In all figures, the calculated points are presented by the corresponding symbols. The connecting lines were obtained by cubic splines, a method which produces the most probable reconstruction of a smooth curve from a fixed number of digitized points [40].

The halorhodopsin photocycle was measured on naturally 2D crystalline samples from overproducing mutant [41] of *Halobacterium salinarium*. The measurements were performed at the Max Planck Institute for Biochemistry (Martinsried, Germany) using a polychromatic time-resolved spectrometer [42] with minor modifications of the measuring procedure. Absorption changes in the visible were monitored simultaneously at 32 wavelengths in time domains from sub- to hundreds of milliseconds with 130 μs time-resolution. The photocycle was excited by 5 ns, 2 mJcm^{-2} flashes of a dye laser at 580 nm, and was monitored by a polychromatic beam of approx. 2 mWcm^{-2} intensity, polarized at the "magic" angle (54°44′) relative to the excitation in order to eliminate photoselection effects. The signal-to-noise ratio achieved after averaging was $\approx$ 1300. The sample, a suspension of membrane sheets in a 5 mM Tris/HEPES buffer at pH 7.0 in the presence of 1 M NaCl, had an optical density of 0.45.

4. Mathematical background

4.1. Description of photocycle dynamics

Consider a general case when the dynamics of a complex chemical/biochemical system is described by a system of coupled linear [2] differential rate equations.The *kinetic scheme* of transformations, the sequence of intermediates and the paths of their interconversions, is fully described by matrix **K**, each element of which, $K(i,j)$, is the true (intrinsic) rate constant for the reaction (decay) from state i into state j. The diagonal elements of **K**-matrix, $K(i,i)$, which have no physical meaning, can be assigned zeros without loss of generality. For example, for a cyclic reaction:

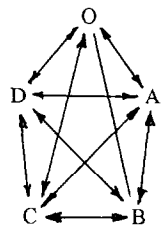

the corresponding matrix $\mathbf{K}(i,j)$ is

$$\begin{Vmatrix} 0 & K_{OA} & K_{OB} & K_{OC} & K_{OD} \\ K_{AO} & 0 & K_{AB} & K_{AC} & K_{AD} \\ K_{BO} & K_{BA} & 0 & K_{BC} & K_{BD} \\ K_{CO} & K_{CA} & K_{CB} & 0 & K_{CD} \\ K_{DO} & K_{DA} & K_{DB} & K_{DC} & 0 \end{Vmatrix}$$

[2] A nonlinear case could be treated in a similar way; this communication focuses on the linear case because it seems to be the case for retinal proteins, cytochrome *c* oxidase, phytochrome, and photoactive yellow protein.

Let us consider a case where at the initial moment $t = 0$ (just before excitation), all the molecules are in state O (in general, prior to excitation they could be distributed through states O, A, B, C and D in equilibrium corresponding to a minimum of the free energy $G = H - S \cdot T$). The studied cycle of transformations is initiated by inputting into the system some additional energy, which drives the system from thermodynamic equilibrium. The object of study is the dynamics of return of the system back to equilibrium. The upper sub-diagonal elements characterize "forward" reactions (e.g. A → B), with the lower sub-diagonal containing the rate constants for "reverse" steps (e.g. A ← B). Including both in the model is absolutely obligatory for any but the most trivial scheme. Non-zero off-tridiagonal matrix elements correspond to branching and short-cuts (e.g. A ⇔ C).

To prohibit *perpetuum mobile*-like spontaneous evolution of the system along some of the closed loops of reaction pathways (e.g. A ⇔ B ⇔ C ⇔ A), the integrated change of free energy, ΔG, along *any* possible close loop must be zero. This leads to the law of detailed balance [43] which imposes restrictions on $K(i,j)$. For instance, for the *sub-cycle* A ⇔ B ⇔ C ⇔ A, it results in

$$K_{AB} \cdot K_{BC} \cdot K_{CA} = K_{AC} \cdot K_{CB} \cdot K_{BA}$$

i.e. not all of the $K(i,j)$ are independent. For a cycle with N_i transient states, plus the initial one, "O", in the above example, this restriction reduces the number of independent $K(i,j)$ from $N_i(N_i + 1)$ to $[N_i(N_i + 3) - 2]/2 + 1$ [8].

Using vector and matrix notation, concentrations of all states at any time, $\mathbf{C}(i,t)$, are described by the equations

$$d\boldsymbol{C}(i,t)/dt = \boldsymbol{M}(i,j) \cdot \boldsymbol{C}(j,t) \quad (1)$$

where $i = 0 \ldots N_i$, with $i = 0$ corresponding to unexcited state, and $i = 1 \ldots N_i$ correspond to transient intermediate states. The matrix of coefficients, $\mathbf{M}(i,j)$, is easily obtained from matrix $\mathbf{K}(i,j)$. For non-diagonal elements, by taking a matrix transpose of $\mathbf{K}(i,j)$

$$M(i,j) = K(j,i) \quad (2a)$$

and for diagonal ones, by substituting the main diagonal's zeros with the corresponding sums

$$M(i,i) = -\sum_{j=0}^{N_i} K(i,j) \quad (2b)$$

The 2D array of experimentally measured time-resolved data, $\Delta\mathbf{A}(\lambda,t)$ arises from a product

$$\Delta\boldsymbol{A}(\lambda,t) = \varphi \cdot \boldsymbol{E}(\lambda,i) \cdot \boldsymbol{C}(i,t) \quad (3)$$

Note that in any experimentally measurable data, differential extinctions, $\mathbf{E}(\lambda,i)$, always appear (pre)multiplied by the "cycling fraction", φ. In a general case, a correct, i.e. not based on *a priori* assumptions of $\mathbf{E}(\lambda,i)$, estimation of φ is a complex problem [44], and recalculation from differential to absolute spectra of intermediates can be ambiguous. Here we will limit ourselves to calculation of the differential spectra.

From the general theory of linear differential equations, the solution of Eq. (1) can be written using eigen-values, $\mathbf{k}^*(j)$, and eigen-vectors, $\mathbf{D}(i,j)$, of the $\mathbf{M}$-matrix

$$\boldsymbol{C}(i,t) = \boldsymbol{D}(i,j) \cdot \exp\{-t \cdot \boldsymbol{k}^*(j)\} \quad (4)$$

Now let us compare Eq. (3) and Eq. (4) with the corresponding output of popular algorithms for analyzing kinetic data.

4.2. Analysis of 2D arrays of kinetic data by GF and SVD

The result of the *global fitting*, GF, approximation is

$$\Delta\boldsymbol{A}(\lambda,t) = \boldsymbol{B}(\lambda,j) \cdot \exp - \{t \cdot \boldsymbol{k}_{GF}(j)\} \quad (5)$$

In the ideal case, GF should converge to a close estimate of the true apparent time constants

$$\boldsymbol{k}^*(j) \approx \boldsymbol{k}_{GF}(j) \quad (6)$$

Combining Eqs. (3)–(5), one gets

$$\boldsymbol{B}(\lambda,j) = \varphi \cdot \boldsymbol{E}(\lambda,i) \cdot \boldsymbol{D}(i,j) \quad (7)$$

for the case of an accurate approximation. The values of $\mathbf{B}(\lambda,j)$ are perturbed when Eq. (6) is poorly satisfied. Note, that even in the case of an accurate approximation, the amplitude spectra of the exponentials are linear combinations of real differential extinctions, $E(\lambda,i)$; the apparent rate constants $\boldsymbol{k}_{GF}$ are

complex algebraic functions from the intrinsic ones (see [1] for more discussion).

The result of the *singular value decomposition*, SVD, is

$$\Delta A(\lambda,t) = \varphi \cdot E(\lambda,i) \cdot C(i,t) = U(\lambda,j) \cdot S(j,i) \cdot V^{T}(i,t) \quad (8)$$

By definition, columns of each matrix, **U** and **V**, are orthonormal. Mathematically, deconvolution of matrix $\Delta\mathbf{A}(\lambda,t)$ into a product of two orthonormal matrixes, **U** and **V**, is not unique, and there are an infinite number of pairs of such orthonormal matrixes which could be obtained from **U** and **V** by rotation [45,46]. The uniqueness of singular value decomposition is determined by an additional restriction: matrixes **U** and **V** are chosen such that reconstruction of the initial matrix, $\Delta\mathbf{A}(\lambda,t)$, with the first N columns of **U** and corresponding N rows of **V** (i.e. setting $S(i,i) \equiv 0$ for $i > N$) produces the best possible approximation of $\Delta\mathbf{A}(\lambda,t)$ in the least squares sense. This reconstruction is then, by definition, superior to any other N-factor approximation by any linear combination of columns of **U** and **V**.

Real intermediate spectra $\mathbf{E}(\lambda,i)$ should hardly be expected to form an orthogonal system, that is to be *completely* linearly independent, but even if they were, there is no mathematical reason why the coordinate system formed by vectors of the **E**-matrix should have the same orientation in parameter space as that of the **U**-matrix. On the contrary, the fact that the first basis spectrum, $\mathrm{U}(\lambda,1)$, represents the best (in the least-squares sense) one-factor approximation of the multi-spectra mixture, forces the SVD algorithm to calculate it as a weighted sum of all components [35]. In the geometrical interpretation, this first basis spectrum corresponds to a multidimensional (hyper)-diagonal, rather than to any particular true spectrum, even when the original (true) spectra are linearly independent (orthogonal). If the true spectra are not linear-independent, the orthonormal set of $\mathrm{U}(\lambda,i)$ vectors could be created (by SVD) from the given set of true spectra only as their linear combinations. As a result (in the general case), the SVD *basis spectra* (columns of the **U**-matrix) are linear combinations of the real differential spectra. Likewise, the corresponding SVD kinetics (columns of the **V**-matrix) are also linear combinations of the true time-dependent concentrations of different intermediates.

The central problem in kinetic data analysis is the deconvolution of the experimentally measured data matrix $\Delta\mathbf{A}(\lambda,t)$ into two factors: true spectra $\mathbf{E}(\lambda,i)$ and concentration kinetics $\mathbf{C}(i,t)$. Once either the **E**- or the **C**-matrix is calculated, the problem is almost completely solved. The temporal behavior in both matrixes $\mathbf{C}(i,t)$ and $\Delta\mathbf{A}(\lambda,t)$ is characterized by the same set of eigen-values, $\mathbf{k}^{*}(j)$, of the **M**-matrix (see Eqs. (4)–(6)), and can be obtained by a direct global fit. However, the $N_i + 1$ eigen-values obtained are not enough to recalculate the $(N_i + 1) \cdot (N_i + 1)$-element **M**- and **K**-matrixes. This becomes possible when the $(N_i + 1) \cdot (N_i + 1)$ matrix of eigen-vectors, $\mathbf{D}(i,j)$ is known, along with corresponding eigen-values [3]. However, $\mathbf{D}(i,j)$ is obtainable when matrix $\mathbf{C}(i,t)$, but not the matrix $\Delta\mathbf{A}(\lambda,t)$, is globally fitted (see Eq. (4), Eq. (5), and Eq. (7)). Thus, *any* set of "true" spectra (assumed, proposed, estimated, guessed, etc.) leads unambiguously to some *particular* kinetic scheme (described by a **K**-matrix). The converse is also true: a transformation matrix for recalculating matrix $\mathbf{E}(\lambda,i)$ from either $\mathbf{B}(\lambda,j)$ or $\mathbf{U}(\lambda,j)$ can easily be constructed if the **K**-matrix is fully known.

Recently, several groups have claimed that experimental data, $\Delta\mathbf{A}(\lambda,t)$, were deconvoluted into true spectra, $\mathbf{E}(\lambda,i)$, and concentration kinetics, $\mathbf{C}(i,t)$, without *a priori* knowledge (or assumption) of a kinetic scheme [5,7,15,19,20], or even in a scheme-independent way [14]. Mathematically, this is impossible. Any recalculation of matrixes $\mathbf{U}(\lambda,j)$ or $\mathbf{B}(\lambda,j)$ into the matrix $\mathbf{E}(\lambda,i)$, is based on some *logical* and/or *physical / chemical* assumptions/restrictions. Thus, recalculations were in fact done in a frame of a particular (*a priori* assumed) kinetic scheme, which is defined by those assumptions in an *implicit* way. A particular photocycle scheme was thus already assumed when $\Delta\mathbf{A}(\lambda,t)$ was decomposed into the two matrixes $\mathbf{E}(\lambda,i)$ and $\mathbf{C}(i,t)$ and, moreover, this scheme can be directly calculated [9]. Conclusions of this type of circular analysis

[3] According to a general theorem a set of eigen-values and eigen-vectors uniquely determines all elements of a matrix: $\boldsymbol{M} = \boldsymbol{D}(\mathbf{1} \cdot \mathbf{k}^{*}) \cdot \boldsymbol{D}^{-1}$, where **1** is the identity matrix.

[5,7,14,15,19,20] are therefore valid only as long as those assumed schemes are correct.

4.3. Analysis of 3D arrays of kinetic data by direct fitting to systems of coupled differential equations

To be able to deconvolute both true spectra, $\mathbf{E}(\lambda,i)$, and concentration kinetics, $\mathbf{C}(i,t)$, from experimentally measured data, $\Delta\mathbf{A}(\lambda,t)$, some additional information is needed beyond that present in the 2D data array. As pointed out by Nagle [8], the necessary information is available in the 3D data array, $\Delta\mathbf{A}(\lambda,t,T)$, measured at at least three different temperatures, provided that individual intrinsic rate constants have a non-degenerate temperature dependence. The analysis is based on an assumption that only the concentration dynamics, $\mathbf{C}(i,t)$, but not the true spectra, $\mathbf{E}(\lambda,i)$, are temperature-dependent [8]. To further simplify the case, let us assume that all intrinsic (rather than apparent) rate constants forming the **K**-matrix obey (at least in a limited temperature range) the Eyring form [47]

$$K(i,j,T) = \{h/(k\cdot T)\} \cdot \exp\{-[\Delta H^{\#}(i,j) - \Delta S^{\#}(i,j)T]\} \quad (9)$$

Using Eq. (9) and Eqs. (2a) and (2b), one rewrites Eq. (1) as

$$d\boldsymbol{C}(i,t,T)/dt = \boldsymbol{M}(i,j,T)\cdot\boldsymbol{C}(j,t,T) \quad (10)$$

Subsequently, Eq. (3) is transformed into

$$\Delta\boldsymbol{A}(\lambda,t,T) = \varphi(T)\cdot\boldsymbol{E}(\lambda,i)\cdot\boldsymbol{C}(i,t,T) \quad (11)$$

Here $\Delta\mathbf{A}(\lambda,t,T)$ is already a 3D array of data. The real experimentally measured 3D array would include some noise, $\delta(\lambda,t,T)$

$$\Delta\boldsymbol{A}_{\text{experiment}}(\lambda,t,T) = \Delta\boldsymbol{A}_{\text{theory}}(\lambda,t,T) + \delta(\lambda,t,T) = \varphi(T)\cdot\boldsymbol{E}(\lambda,i)\cdot\boldsymbol{C}(i,t,T) + \delta(\lambda,t,T) \quad (12)$$

Assuming that the noise, $\delta(\lambda,t,T)$, is random white noise, an unbiased estimate of **E** and **C** by least squares can be obtained

$$RSMR = \Sigma\Sigma\Sigma\{\Delta\boldsymbol{A}_{\text{experiment}}(\lambda,t,T) - \varphi(T)\cdot\boldsymbol{E}(\lambda,i)\cdot\boldsymbol{C}(i,t,T)\}^2 \to 0 \quad (13)$$

Mathematically, the problem involves both *non-linear*, $\Delta H^{\#}(i,j)$ and $\Delta S^{\#}(i,j)$, and *linear*, $\mathbf{E}(\lambda,i)$, parameters. Applying the variable projection mechanism [31,48], one can subdivide this problem into nonlinear least squares in the space of nonlinear parameters [4], and the corresponding linear least squares. Only the nonlinear part is solved by iterations, while linear least squares can be solved without them. Thus, current estimates for $\Delta H^{\#}(i,j)$ and $\Delta S^{\#}(i,j)$ are obtained iteratively by some search algorithm. Then the **K**-matrix is calculated according to Eq. (9), the **M**-matrix according to Eqs. (2a) and (2b), and the **C**-matrix according to Eq. (4). The corresponding estimates for the spectra $\mathbf{E}(\lambda,i)$ (to be more exact, the product of $\varphi(T_0)\cdot\mathbf{E}(\lambda,i)$) [5] are obtained by solving the following system of algebraic equations

$$\boldsymbol{E}(\lambda,i)\cdot\boldsymbol{P}(i,j) = \boldsymbol{R}(\lambda,j) \quad (14)$$

where the **P**- and **R**-matrixes are

$$P(i,j) = \sum_T\sum_t\{\varphi(T)C(i,t,T)C(j,t,T)\} \quad (15)$$

$$R(\lambda,j) = \sum_T\sum_t\{\Delta A(\lambda,t,T)C(j,t,T)\} \quad (16)$$

Differential extinction spectra, $\mathbf{E}(\lambda,i)$, for all transient intermediates are obtained by solving Eq. (14) separately at each wavelength/wavenumber.

5. Phenomenological approximation of time-resolved data by global fitting and singular value decomposition

The aim of kinetic data analysis is to decompose the measured array of data, $\Delta\mathbf{A}(\lambda,t)$, into time-independent spectra and wavelength-independent kinetics. This decomposition is not unique. A full treatment involves several steps. The first (obligatory) step is to determine the number of transient states which give rise to the observed kinetics. The second

[4] The number of non-linear parameters is twice the number of allowed transitions included in the model, i.e. a pair of $\Delta H^{\#}$ and $\Delta S^{\#}$ for each non-zero element in **K**-matrix.

[5] Let $\varphi(T_0)$ be the fraction cycling at one particular temperature. The scaling factors, $\varphi(T_i)/\varphi(T_0)$ could be calculated in a similar way, based on the same assumption that the differential spectra, $\mathbf{E}(\lambda,i)$, are temperature-independent (see Section 6.2 for more details).

(optional) step is to find a *phenomenological* description of the experimentally measured data within experimental error. That is, to approximate data by *apparent* kinetics, and to compute the apparent time constants and amplitudes. The final (desirable) step is to extract *intrinsic* rate constants and differential extinctions of all transient states.

The GF analysis of kinetic data is based on the *a priori* assumption on the mechanism of involved reactions (for instance, first-order or pseudo-first-order, second-order reactions, etc.). This *a priori* information is used to assume that the apparent kinetics at each measured wavelength/wavenumber, $\Delta A(\lambda,t)$, can be expanded into a series of certain time-dependent functions, $\Sigma\{B(\lambda,j)f(j,t)\}$. For instance, for first- or pseudo-first-order reactions, $f(j,t)$ are exponentials, the most widely used set of time-dependent functions in GF. The important assumption is that this time-series expansion has a finite number of terms, $j = 1 \ldots N_c$, (which is equal to the number of transient states in the kinetic scheme, i.e. $N_c = N_i$, according to a general theorem of the theory of differential equations) [6]. The time-dependent factors, $f(j,t)$, are wavelength/wavenumber-independent. Only their apparent amplitudes, $B(\lambda,j)$, are wavelength/wavenumber dependent. The fitting is performed iteratively in the N_c-dimensional space of the N_c nonlinear parameters, $k_{GF}(j)$, while the matrix of linear coefficients, $\mathbf{B}(\lambda,j)$, is obtained by directly solving of a *linear least squares* problem. The performance of several custom-built versions of GF programs were reported in the literature (see, for instance, [1,3,12,21,29,31,32,49,50]).

Contrary to a widespread belief that one can always fit a given set of data, $\Delta\mathbf{A}(\lambda,t)$, with either N_c or $N_c + 1$ exponentials, there is a *statistically significant* number of exponentials needed and sufficient for a description of the data. This number can be readily (and exactly) determined by applying simple statistical tests [51,52], the F-test in particular. A clear-cut conclusion from F-test statistics for the number of intermediates *detected* in experiment (rather than on the fitting stage) is an apparent advantage of the application of GF to time-resolved data analysis (see also [2]).

SVD provides a unique deconvolution of original data, $\Delta\mathbf{A}(\lambda,t)$, into the product of three orthonormal matrixes $\mathbf{U}\cdot\mathbf{S}\cdot\mathbf{V}^{\mathbf{T}}$ [34,40]. When applied to time-resolved measurements, the **U**-matrix contains *basis spectra*, and the **V**-matrix contains corresponding kinetics (time-course) of these *basis spectra*. The square **S**-matrix contains non-zero elements only on its diagonal. For a noiseless data matrix $\Delta\mathbf{A}$, the number of transient states, N_i, which gives rise to the observed kinetics, $\Delta\mathbf{A}(\lambda,t)$, is equal to the *rank* of the **S**-matrix, and $N_{SVD} = N_i$. The diagonal elements of the **S**-matrix, $S(i,i)$ are non-zero only for $i \le N_i$, and are equal to zero for $i > N_i$ (i.e. $N_{SVD} \equiv N_i$). For cases when some noise is present, as in any experimental data set, *proliferation of experimental errors* [46,53] leads to non-zero $S(i,i)$ even for $i > N_i$. That is, the rank of the **S**-matrix is different from N_i. To separate the signal from noise, one needs to determine the number of statistically significant components N_{SVD}. There are several ways to determine N_{SVD} [35,40,46,54,55], none of which are completely reliable. Among the most widely used statistical criteria for evaluation of N_{SVD} are

· Autocorrelations in matrices **U** and **V** [35,56]

$$\mathrm{Ac}\{\boldsymbol{U}(j)\} = \sum_{i=2}^{N_\lambda} U(i-1,j)U(i,j) \tag{17}$$

$$\mathrm{Ac}\{\boldsymbol{V}(j)\} = \sum_{i=2}^{N_\lambda} U(i-1,j)U(i,j) \tag{18}$$

· Comparison of the corresponding sum of *singular values*, $S(i,i)$, to the noise level. A correct estimate of N_{SVD} should satisfy the following inequality [35,56]

$$\sum_{i=N_{SVD}+1}^{N} s^2(i,i) \le \sum_{\lambda,t} \sigma_\delta(\lambda,t) < \sum_{i=N_{SVD}}^{N} s^2(i,i) \tag{19}$$

· Special indication functions: e.g. (i) the Brown–Donahue fractional indicator [55]

$$\mathrm{FRAC}(j) = s^2(j) / \sum_{i=j}^{N} s^2(i) \tag{20}$$

[6] This is true for a non-degenerate case, i.e. when no two apparent rates constants are exactly equal to one another. The true degenerate case is important for mathematics, but practically irrelevant for chemical kinetics since this might happen only in a very narrow range of temperature, due to the difference in temperature dependencies of particular rate constants.

or (ii) that of Malinowski [54]

$$\mathrm{IND}(j) = \sqrt{\frac{\sum_{i=j+1}^{N} s^2(i,i)}{N_\lambda (N_t - j)^5}} \qquad (21)$$

The former reaches its minimum at $j = N_{SVD} + 1$, the latter at $j = N_{SVD}$.

Mathematically, determination the value of N_{SVD} is the equivalent to an estimation of how experimental noise has affected the rank of the **S**-matrix. Since SVD is a rank-*reducing* rather than rank-*determining* procedure [34,40], this is an extremely nontrivial problem.

Suppose now that two transient states have similar (but not equal) spectra. Their linearly independent *basis spectra* are going to be their *sum* and their *difference*. The latter is going to be considerably smaller than other basis spectra. In the case of SVD analysis, this corresponds to a smaller singular value $S(i,i)$, which might be easily mixed with noise components, and therefore disregarded in the subsequent analysis. Autocorrelation analysis [35,38,56] of corresponding rows/columns sometimes detects such cases, but there is no general way to detect when SVD constructs only one (sum) basis spectrum out of two separate but spectrally similar ones. Mathematically, estimating the number of spectrally distinct forms involved is the problem of determining the rank of matrix $\Delta\mathbf{A}$. SVD is a powerful rank-reducing algorithm, and in any but artificially "noiseless" cases its efficiency in reducing the rank is in direct conflict with the researcher's desire to use it for rank determination.

In practice this is a common feature, when multi-exponential refitting of the first N_{SVD} statistically significant columns of a **V**-matrix produces more than N_{SVD} ($N_{SVD} + j$, $j \geq 1$) statistically significant exponentials [14,19,20,26–28]. This apparent paradox is convincing evidence that a *statistically significant* component was thrown away due to an error in **S**-matrix rank determination (for discussion see also Refs. [17,35,38]). This is a typical case of *misuse* of a particular numeric algorithm, rather than an illustration of its inherent weakness.

To illustrate the *pros* and *cons* of GF and SVD, let us apply both methods to a set of synthetic data, for which both the $\mathbf{E}(\lambda,i)$ and the $\mathbf{C}(i,t)$ matrices are known. For this purpose, a series of $\Delta\mathbf{A}(\lambda,t)$ "data" sets were generated using one and the same pair of $\mathbf{E}(\lambda,i)$ and $\mathbf{C}(i,t)$ matrixes, but with different amounts of *white* noise, $\delta(\lambda,t)$ (added by a random number generator with a known dispersion σ_δ). The true intermediates' differential spectra, $\mathbf{E}(\lambda,i)$, used for simulations are shown in Fig. 1. The cycle was assumed to have the following kinetic scheme

$$O \Rightarrow A \rightarrow B \Leftrightarrow C \Leftrightarrow D \rightarrow O \qquad (22)$$

The sample was assumed to have an optical density of 1 OD at its maximum, and 30% of the molecules were assumed to be excited into the photocycle (photoconversion of 30%). This kinetic scheme (Eq. (22)) was assumed to be characterized by the following **K**-matrix (in s^{-1})

$$\begin{Vmatrix} 0 & h\nu & 0 & 0 & 0 \\ 0 & 0 & 600 & 0 & 0 \\ 0 & 0 & 0 & 69.4 & 0 \\ 0 & 0 & 9.43 & 0 & 270 \\ 12.6 & 0 & 0 & 25.3 & 0 \end{Vmatrix}$$

The first step, denoted in the above matrix by "$h\nu$", is a light-induced transition from state "O" to state "A". This is considered instantaneous, so the initial conditions are: $C_A(t=0) = \varphi = 0.3$, $C_{B,C,D}(t=0) \equiv 0$. The cycle involves four transient states (A, B, C, D), interconnected by six non-zero intrinsic

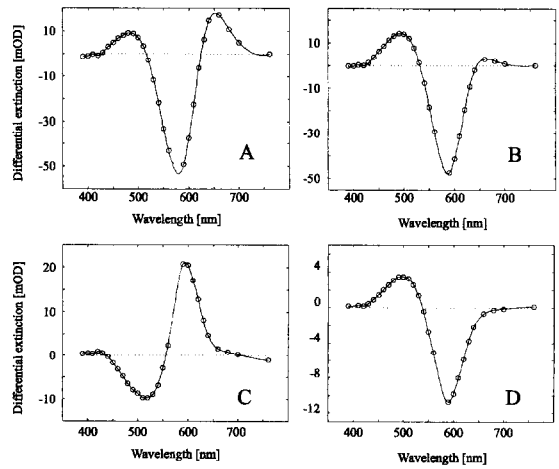

Fig. 1. A set of synthetic spectra for intermediates A, B, C, and D, interconnected according to a kinetic scheme of Eq. (22). These spectra were used for all further simulations.

rate constants, listed in the **K**-matrix. Using Eqs. (2a) and (2b), it can be rewritten into the **M**-matrix of coefficients of coupled rate equations in the form of Eq. (1). Thus, the apparent kinetics are characterized by four exponentials (plus a constant level), corresponding to the vector of eigen-values (in s^{-1})

$$\boldsymbol{k}^* = [600, 307, 68.0, 11.30] \quad (23)$$

Back reactions in both local equilibria, B ⇔ C and C ⇔ D, were chosen to provide detectable, but yet not too pronounced effects (corresponding equilibria constants are 7.4 and 10.7). The kinetics of the true concentrations is presented in Fig. 2. The spectra and numerical values for intrinsic rate constants were chosen in such a way that the simulated spectral data, $\Delta\mathbf{A}(\lambda,t)$, closely correspond to those observed for the real case of halorhodopsin (a natural photoreactive protein from *Halobacterium salinarium*).

To provide a handy measure of the added noise, we shall define the signal-to-noise ratio, S/N, as the ratio of the biggest transient amplitude (in the whole 2D array), $max\{\Delta\mathbf{A}(\lambda,t)\}$, to noise dispersion, σ_δ

$$S/N = \max\{\Delta\boldsymbol{A}(\lambda,t)\}/\sigma_\delta \quad (24)$$

"Data" arrays with S/N in the range from 160 to $6 \cdot 10^4$ (i.e. noiseless within 16-bit accuracy) were generated for testing both GF and SVD. Fig. 3 presents two such sets of simulated data: (i) "without noise" in Fig. 3a, and (ii) with S/N = 320 in Fig. 3b. The global fitting program *FITEXP* was applied to the 2D arrays (like those in Fig. 3a and b) subsequently with 2, 3, 4, and 5 exponentials. F-test statistics [51,52] revealed 4 statistically valid exponentials for arrays of data with S/N ≥ 250 (see Fig. 4a and b). For lower S/N values, the noise level was too high for extraction of all four exponentials. Thus, for S/N ≥ 250, *FITEXP* (GF) was able to correctly and unambiguously calculate the number of transient states, N_i, giving rise to the observed apparent kinetics, $\mathbf{A}(\lambda,t)$. Thus, the first obligatory step of any kinetic analysis was correctly performed. Note that the numerical value for the threshold value of S/N which allows extraction of a specific number of exponentials, N_e, from a given array of experimental data, is extremely sensitive to the difference/likeness in the shape of differential spectra, $\mathbf{E}(\lambda,i)$, of the intermediates involved. In this synthetic example, the intermediates' spectra were assumed to overlap strongly with the closely similar differential spectra (see Fig. 1). The value of S/N ≥ 250, needed for extraction of the four exponentials, could be used as an estimate for the case of the halorhodopsin photocycle, given the similarity of simulated data, $\Delta\mathbf{A}(\lambda,t)$, with experimentally measured curves for its photocycle. Much lower S/N values might be sufficient if the differences in spectra are more pronounced (see for instance Refs. [1,2]). Earlier, the same program, *FITEXP*, was used to successfully extract up to six exponentials from flash photolysis data for the bacteriorhodopsin photocycle [12].

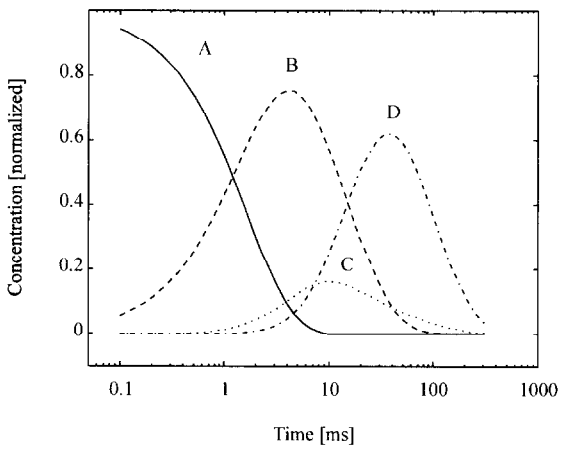

Fig. 2. Assumed true concentrations of the four intermediates: A, solid; B, dashed; C, dotted; D, dash-dotted lines at 20°C for the model of Eq. (22).

In the case of "noiseless" data, the RSMR value is equal to the computational round-off error, and, therefore, numeric values of the fitted (apparent) rate constants, $\mathbf{k}_{GF}$, are in excellent agreement with the true values of the corresponding eigen-values, $\mathbf{k}^*$. The same excellent agreement was obtained for the amplitudes, $\mathbf{B}(\lambda,j)$, in the sense of Eq. (7). The errors in both $\mathbf{k}_{GF}$ and **B**, of course, increase with decreasing signal-to-noise ratio. For instance, for the data array with S/N = 320, *FITEXP* extracts four exponentials, $\mathbf{k}_{GF}$, in close agreement with the true values (corresponding eigen-values, $\mathbf{k}^*$, compare to Eq. (23))

$$\mathbf{k}_{GF} = [532, 342, 68.5, 11.30] \quad (25)$$

F-test statistics clearly indicates that four and only four exponentials are statistically valid. The risk

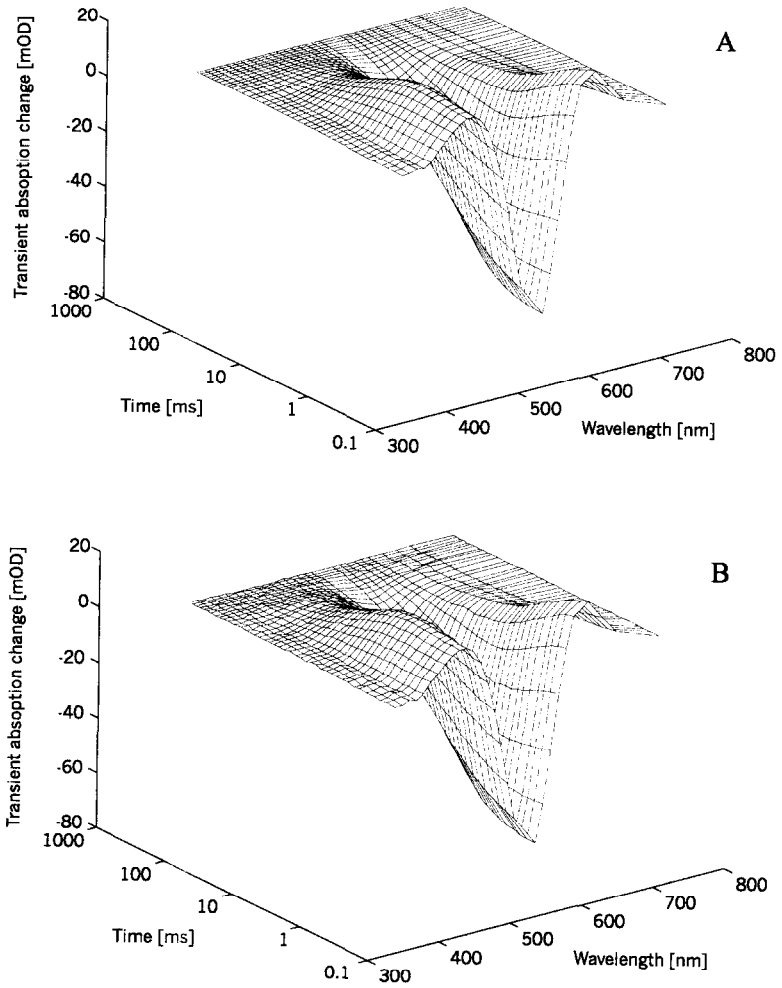

Fig. 3. Synthetic transient absorption changes obtained for the photocycle, resulting from the kinetics (Fig. 2) of the intermediates in Fig. 1: A, noiseless data; B, data with added white noise with S/N = 320.

value (at S/N = 320) of erroneous addition of an extra exponential is below 0.05% for addition of the 4th exponential, but increases to 95.1%, when the validity of addition of the 5th exponential is considered. This clearly indicates that the fourth exponential is statistically significant, but not the fifth. Amplitude spectra, $\mathbf{B}(\lambda,j)$, obtained from GF (by *FIT-EXP*) approximation of data arrays for the 4-exponential fit are presented in Fig. 4.

The same synthetic data were also subjected to SVD analysis. In the case of "noiseless" data, statistical criteria (Eqs. (17)–(21)) unanimously and unambiguously indicate the presence of four different basis spectra, **U**, and the corresponding four kinetic components, **V**. Fig. 5 presents the first four (statistically valid) columns of both matrixes, **U** and **V**. In the case of "noiseless" data, SVD analysis thus produces a correct estimate of the number of states involved, N_i. However, this procedure breaks down more rapidly than the GF method when the level of noise increases. Fig. 6 presents the first four columns of **U** and **V** matrices for S/N = 320. At this S/N value, all statistical criteria (Eqs. (17)–(21)) unambiguously indicate that only the first three components are statistically valid: Ac{**U**(4)} = 0.35, Ac{**V**(4)} = 0.29, far below the 0.6 threshold recom-

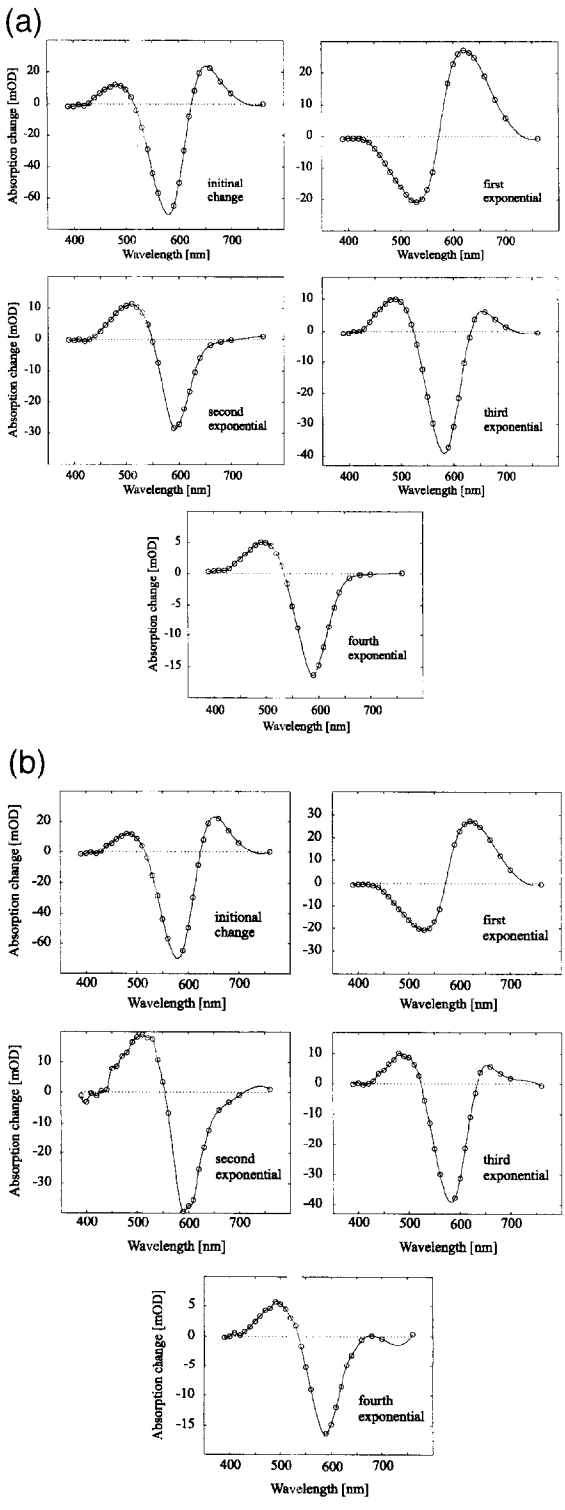

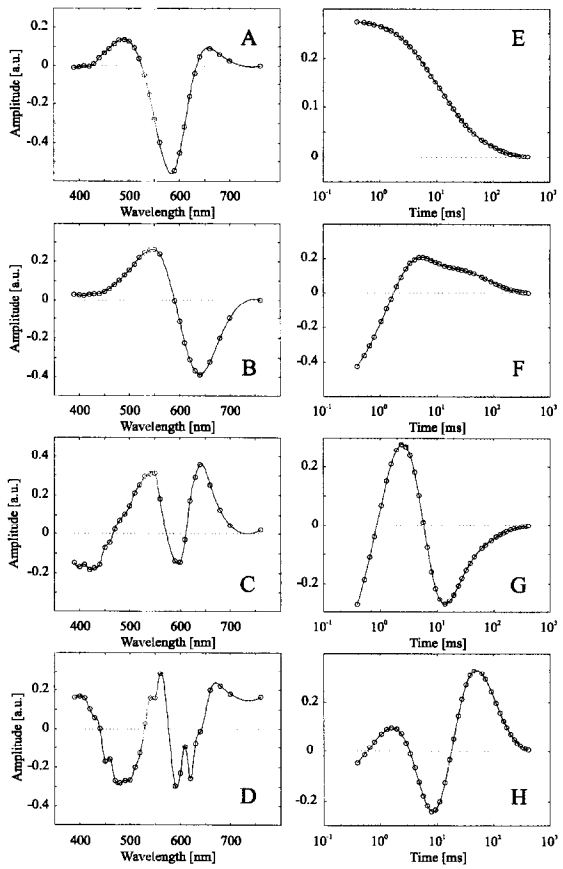

Fig. 5. Results of SVD analysis of noiseless data from Fig. 3a. The first four basis spectra, $\mathbf{U}(\lambda,i)$ (A–D), and their corresponding kinetics, $\mathbf{V}(t,i)$ (E–H).

mended by the author of these autocorrelation tests [35,56], while the corresponding values for the first three components are 0.78–0.92 and 0.70–0.96. The inequality in Eq. (19) is fulfilled for $r = 3$; the FRAC(j) function (Eq. (20)) reaches its minimum at $j = 4$, indicating only three valid components [55]; the IND(j) function reaches its minimum at $j = 3$. Thus, all criteria declare the fourth component statistically insignificant. Comparing the cases of "noiseless" data and S/N = 320, it can be seen that the increase in noise level leads to a complex proliferation of errors to the extent that SVD produces con-

Fig. 4. Amplitude spectra, $\mathbf{B}(\lambda,i)$ for multi-exponential fitting of data in Fig. 3 by the GF program *FITEXP*: (a), noiseless data; (b), data with added white noise with S/N = 320.

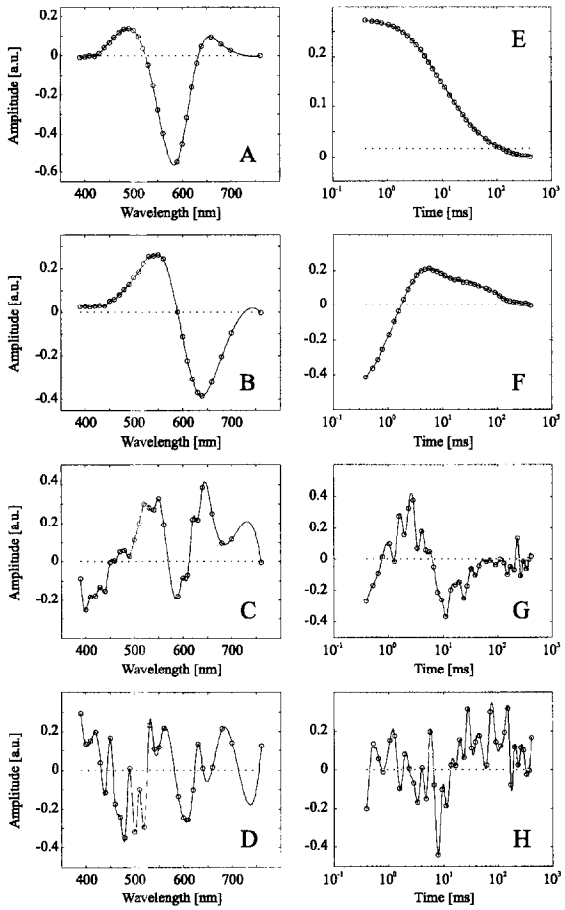

Fig. 6. Results of SVD analysis of data with S/N = 320 (from Fig. 3b). The first four basis spectra, $\mathbf{U}(\lambda,I)$ (A–D), and their corresponding kinetics, $\mathbf{V}(t,i)$ (E–H).

fusing results, being unable even to determine the number of transient states involved. Note that the signal-to-noise level is still higher than in most kinetic studies routinely reported in the literature, while similarity in the intermediates' spectra is no more pronounced than for the published spectra of the distinct intermediates of bacteriorhodopsin [3,4,7,15,57], halorhodopsin [19,20,58], or phytochrome [26].

Simultaneous (global) refitting of the first three components of the **V**-matrix with multi-exponentials and subsequent analysis by F-test produce conclusive evidence, that four, rather than three, kinetic components, and therefore four intermediates, are present in the synthetic data array with S/N = 320. Similar situations, when global refitting of the first N_{SVD} components (or a full array of data reconstructed with $S(i,i) = 0$ for $i > N_{SVD}$) produces a number of exponentials in excess of the number of basis spectra used, were reported [14,17,19,20,26–28]. In most cases, an assumption was made that two or more intermediates share one and the same spectrum and should be *consecutive* (e.g. B and C) in the kinetic scheme. These "spectrally indistinguishable" states were then treated as a "sum of states", with a single concentration kinetics assigned to it [9,19,20]. [7] Our example (Eq. (22) and Fig. 1) illustrates a case when this logic leads to a false conclusion: the spectrally similar intermediates are 'B' and 'D' (see Fig. 1) with a distinctly different intermediate 'C' in between. Treating intermediates 'B' and 'D' as two states in fast direct balance would lead to a model in which state 'C' is misplaced and its spectrum miscalculated, as well as practically all corresponding concentrations.

Both the GF and SVD produce a best (in the least squares sense) phenomenological approximation of data $\Delta\mathbf{A}(\lambda,t)$. The fact that GF with sufficient accuracy detects and characterizes all four intermediates at S/N = 320, points out that at this noise level *all four* intermediates are both kinetically and spectrally distinguishable.

To highlight the truly *fundamental* limitations of both GF and SVD, let us compare the results of application of both methods to noiseless data sets. In this case both GF and SVD provide a four-term or four-factor approximation accurate within the round-off error. The fitted kinetics, $f(j,t)$ from GF or $\mathbf{V}(t,j)$ from SVD, is a sum of exponentials, with rate constants corresponding to the eigen-values, $\mathbf{k}^*$, of the **M**-matrix. Thus, the kinetics are fully approximated by only four exponential components, while there are six non-zero elements in the **M**-matrix. Most illustrative is a comparison of the true spectra used for the simulations, $\mathbf{E}(\lambda,i)$, (Fig. 1), with exponential amplitudes of the GF, $\mathbf{B}(\lambda,i)$, (Fig. 4a) and the basis spectra, $\mathbf{U}(\lambda,i)$, of SVD (Fig. 5a). These three sets of spectra are really different: both GF and SVD generate spectral components, which cannot be

[7] A case when those states are not consecutive in kinetic scheme was also discussed recently [17].

associated directly with true differential spectra. Thus, both GF and SVD provide only a phenomenological description: both $\mathbf{B}(\lambda,i)$ and $\mathbf{U}(\lambda,i)$ are still linear combinations of the true spectra, in a sense no more informative than any stroboscopic time-slice at some particular time-delay after the flash. This simple fact has been accepted about GF results for many years [1], but is still regularly challenged by some proponents of SVD analysis.

6. *SCHEMEFIT*—a program for fitting 3D arrays of spectra-kinetic data to a system of coupled differential rate equations

6.1. General features of SCHEMEFIT

As was shown in the previous section, the 2D data array does not contain enough information for unambiguous evaluation of a full kinetic scheme with intrinsic rate constants and true intermediate spectra. As was pointed out earlier [8], the insufficient information in a 2D data array can be compensated if a third dimension, for instance temperature, is added to the experimentally measured data. Implementation of this approach is based on the following four assumptions:

1. All intrinsic (microscopic) rate constants for elementary transitions between states (e.g. K_{BC} or K_{BD}) are pseudo-first-order, and, therefore, the photocycle is described by a system of coupled linear differential rate equations [8] (Eq. (1)).
2. In a limited temperature range, all microscopic (intrinsic) rate constants have an Arrhenius-like temperature dependence according to Eyring's transition state theory (Eq. (9)). [9]
3. Activation energies, $\Delta H^{\#}(i,j)$, are different for different microscopic steps, and the **K**-matrices at different temperatures are linearly independent.
4. The true intermediate spectra, $\mathbf{E}(\lambda,i)$, are invariant with temperature. Hence, all temperature dependence in the measured data, $\Delta\mathbf{A}(\lambda,t,T)$, comes from the complex pattern of temperature-dependent kinetics of true concentrations, $\mathbf{C}(i,t,T)$, which is in turn due to the Arrhenius temperature dependence (Eq. (9)) of the microscopic rate constants.

The basic mathematics behind this approach is outlined in Eqs. (9)–(16) of Section 4. The *input* for this analysis consists of three different parts:

1. *Data*: an experimentally measured 3D array (in time, wavelength/wavenumber, and temperature).
2. *Parameter*: the number of transient states detected experimentally. This value is determined by a combination of GF procedure and statistical tests by applying both to 2D data sets, measured at particular temperatures. [10] As shown above, this is an experimentally determined parameter, rather than an additional assumption.
3. *Hypothesis*: a list of microscopic steps which are prohibited (if any) in this particular kinetic scheme (i.e. a list of elements in the **K**-matrix which are always zero). Effectively, this provides a qualitative outline of a kinetic scheme: a sequence of intermediates with a list of allowed transitions, a list of non-zero elements in the **K**-matrix, but without any assumptions or restrictions on their numeric values.

The hypothesis to be tested is a voluntary choice, since *a priori* even a 3D set of experimental data, $\Delta\mathbf{A}(\lambda,t,T)$, provides no *direct* information on the kinetic scheme. Note, that no *a priori* assumptions concerning intermediate spectra or intrinsic rate constants are required or allowed. Moreover, the 3D scheme-fitting analysis will yield a set of calculated differential spectra and corresponding intrinsic rate constants for *any* scheme which does not violate the law of detailed balance [43].

[8] Higher order reactions, e.g. second order, could be treated in a similar way, by changing matrixes **K** and **M**, with subsequent changes in Eq. (2a). Only the case of pseudo-first-order reactions will be considered in this communication.

[9] This assumption is not obligatory (see [8]). However, the current version of the *SCHEMEFIT* was designed for the particular case when this assumption is valid, and only this case will be considered here.

[10] GF/statistical test analyses are done subsequently on each 2D sub-set of data measured at a particular temperature. Cross-comparison (at different temperatures) provides either additional support for the given numeric value of $N_i \equiv N_{GF}$, (when the calculaed value for N_{GF} is temperature-independent), or, otherwise, allows diagnosis of such problems in the experimental data array as outliers (noise bursts), badly chosen measuring time windows, insufficient averaging, etc.

The *output* of the scheme-fitting analysis contains the following information:

1. Intrinsic (microscopic) rate constants for all allowed transitions.
2. Pure differential spectra of all intermediates.
3. Thermodynamic activation parameters, $\Delta H^{\#}(i,j)$ and $\Delta S^{\#}(i,j)$, for all allowed transitions, i.e. the temperature dependence of the intrinsic rate constants.
4. The free energy difference, ΔG, between any two intermediates for which both forward and back reactions were included in the kinetic scheme: $\Delta G_{ij} = \Delta H_{ij} - T\Delta S_{ij} = \{\Delta H^{\#}(i,j) - \Delta H^{\#}(j,i)\} - T\{\Delta S^{\#}(i,j) - \Delta S^{\#}(j,i)\}$. Changes in free energy, ΔG, in the course of the intermediates' transformations provide information on the overall energetics, while pronounced changes in enthalpy, ΔH_{ij}, and entropy, ΔS_{ij}, signal major dissipation and conformation-perturbing steps in the system's dynamics.

All obtained values are valid only in the frame of a particular hypothesized kinetic scheme, which was assumed for the analysis. Hypothesizing different schemes will lead to different combinations of spectra, kinetics and thermodynamic constants. Many, rather than a single kinetic scheme, should be tested against any 3D set of experimental data. The main and the only selection criteria are chemically/physically *sensible* results. The non-negativity of the resulting absolute absorption spectra is probably the strongest criterion. It allows rejection of tentative schemes which lead to intermediate differential spectra with strong negative absorbance outside of the main absorption band of the parent chromophore. Numeric values for the intrinsic rate constants and/or thermodynamic parameters provide further criteria. An unreasonably fast (e.g. femtosecond) calculated rate constant for transitions requiring a major protein conformational change, or a free energy change between intermediates exceeding the overall energy input for excitation of the studied reactions [11], are examples which provide grounds for rejection of a particular kinetic scheme under consideration.

As usual in statistics, a particular kinetic scheme can be rejected but cannot be proved. In a general case, the scheme-fitting analysis of a particular 3D data set normally allows only prediction of a "family" of *favorable* kinetic schemes, without being able to unambiguously choose a single *best fitting* scheme (see [9,13,17] for examples). This latter task, a reduction from several favorable to a single best-fitting scheme, may be further achieved by adding one more dimension, the fourth one, to the experimental data array (e.g. a pH, ionic strength, or other chemical agent dependence). As a by-product, this approach will yield more unique information, such as pK_a or salt-affinity constants for intrinsic rate constants. This information cannot be extracted by other methods.

6.2. The structure of the SCHEMEFIT program

Based on the ideas of the variable projection mechanism [31,48], the fitting procedure in *SCHEMEFIT* is effectively subdivided into two parts: (i) a non-linear least-squares part, and (ii) a linear least-squares part. The former is solved by an iterative quasi-random search in the space of non-linear fitting parameters, $\Delta H^{\#}(i,j)$ and $\Delta S^{\#}(i,j)$. Once a current estimate for $\Delta H^{\#}(i,j)$ and $\Delta S^{\#}(i,j)$ is obtained, the linear least squares is solved without iterations. As a result, differential spectra, $\mathbf{E}(\lambda,i)$, for this given set of $\Delta H^{\#}(i,j)$ and $\Delta S^{\#}(i,j)$ are produced, and the residual sum of squares, RSMR, between the measured kinetics and current approximation, is calculated.

In each step of the iteration procedure, *SCHEMEFIT* subsequently performs the following steps:

1. An initial estimate of the thermodynamic activation parameters ($\Delta H^{\#}(i,j)$ and $\Delta S^{\#}(i,j)$) for each of the $i \rightarrow j$ steps allowed by the kinetic scheme is produced by a random value generator such that the corresponding values of activation free energy, $\Delta G^{\#}$, are within the specified range.
2. All non-zero individual intrinsic rate constants in **K**-matrixes are calculated according to Eq. (9), separately for each temperature.
3. **M**-matrixes (for different temperatures) are recalculated from **K**-matrixes according to Eqs. (2a) and (2b).
4. Eq. (1) is solved numerically (in the form of Eq.

[11] To be more exact, that exceeding the amount stored in the primary act.

(4)), separately for each temperature, using a set of procedures for handling eigen-value-problems, to yield a current approximation of the intermediates' concentration kinetics, $\mathbf{C}(i,t,T)$, for all intermediates at all time points and temperatures.

5. Once the matrix $\mathbf{C}(i,t,T)$ is estimated, the non-linear part of the least squares problem of Eq. (13) is finished, and the current values for extinction coefficients, $\mathbf{E}(\lambda,i)$, are calculated from Eq. (14) as a linear least squares problem in the following three steps.
6. First, the products $\varphi(T) \cdot \mathbf{E}(\lambda,i)$ are calculated separately for all temperatures, T_i, from Eq. (14), using reduced (without summation over temperatures) forms of Eq. (15) and Eq. (16).
7. Second, the scaling factors $\varphi(T_i)/\varphi(T_0)$ are calculated, based on the assumption that extinction coefficients, $\mathbf{E}(\lambda,i)$, are temperature invariant.
8. Third, the extinction coefficients, $\mathbf{E}(\lambda,i)$, are calculated from Eq. (14) using the full Eq. (15) and Eq. (16).
9. When both the spectra, $\mathbf{E}(\lambda,i)$, and kinetics, $\mathbf{C}(i,t,T)$, are known, the residual sum of squares, RSMR, between the measured signal, $\Delta\mathbf{A}_{\text{experiment}}(\lambda,t,T)$, and its current theoretical approximation, $\Delta\mathbf{A}(\lambda,t,T) = \varphi(T) \cdot \mathbf{E}(\lambda,i) \cdot \mathbf{C}(i,t,T)$, is calculated and its value is used as a criterion for goodness-of-fit.
10. The iteration procedure is further performed, repeating each time steps 2 to 9 and substituting the initial step #1 by the following step #11.
11. On each iteration step, new values for $\Delta H^{\#}(i,j)$ and $\Delta S^{\#}(i,j)$ are calculated using the *adaptive random search* algorithm [59]. In short, each new value is calculated from the corresponding value from the previous iteration step in such a way that their difference is a normally distributed random value with a given dispersion, $\sigma_{\Delta S(i,j)}$ or $\sigma_{\Delta H(i,j)}$. When all new values of $\Delta H^{\#}(i,j)$ and $\Delta S^{\#}(i,j)$ are calculated, steps #2–#9 are repeated. If this procedure leads to an improvement in RSMR value, the shift from "old" to "new" $\Delta H^{\#}(i,j)$ and $\Delta S^{\#}(i,j)$ values is accepted; if the RSMR value is increased, the shift is rejected.

As shown above, a single iteration step includes nine sub-steps: #11 and #2–#9, with #11 substituted by #1 on the initial iteration step. The adaptive feature of this algorithm allows changing individual values of $\sigma_{\Delta S(i,j)}$ and $\sigma_{\Delta H(i,j)}$ in the course of iterations. They are increased or decreased by a factor α, based on whether the absolute value of the difference between $\Delta H^{\#}(i,j)_{\text{new}}$ and $\Delta H^{\#}(i,j)_{\text{old}}$ is higher or lower than the corresponding $\sigma_{\Delta H(i,j)}$ value [59]. The "volume" (a product of all σ's) of $\sigma_{\Delta S(i,j)}$ and $\sigma_{\Delta H(i,j)}$ is renormalized each time to prevent its premature decrease, which might lead to sliding into a local minimum.

The flow of the search algorithm is governed by four adjustable parameters: N_{fit}, α, β, and γ. The iterative procedure is repeated for a given set of $\sigma_{\Delta S(i,j)}$ and $\sigma_{\Delta H(i,j)}$ values until a stage is reached, when N_{fit} continuous subsequent attempts to generate new sets of nonlinear fitting parameters, $\Delta H^{\#}(i,j)$ and $\Delta S^{\#}(i,j)$, do not produce any improvement in RSMR. At this point, the set of $\sigma_{\Delta S(i,j)}$ or $\sigma_{\Delta H(i,j)}$ is decreased as a whole by a factor β. The full fitting search is stopped after this step-wise decrease has been performed γ times. Such step-wise decrease in the search space allows an increase in the speed of conversion on later stages of fitting.

The four parameters: N_{fit}, α, β, and γ, permit fine-tuning of the search procedure, balancing between a fast conversion to a local minimum (when N_{fit} and γ are too small while α and β are too big), and an opposite case, which leads to unreasonable computational times without noticeable improvement. As acknowledged even in CERN (European Atomic Energy Center, Switzerland) library documentation [60], there is no *universal* way to fine-tune a search procedure, which is to search for a global minimum on an arbitrary multidimensional surface with local minima. However, a tuning for a particular purpose is possible. *SCHEMEFIT* was tuned on a set of synthetic data imitating the flash-induced signals from retinal protein dynamics. Based on our experience with synthetic curves, the following numeric values were used. The parameter N_{fit} increases exponentially with the number of non-linear fitted parameters. For the case of 10–12 nonlinear parameters (i.e. 5–6 allowed transitions), $N_{\text{fit}} \approx 10^6$ was found optimal, with parameters α, β and γ of 1.04, 2.5 and 5 correspondingly.

As revealed by tests on synthetic data sets, the search in multidimensional space of non-linear fit-

ting parameters is performed over the RSMR surface, characterized by numerous local minima. Therefore, most of the popular search algorithms, which actually search towards a local, rather than the global minimum [60], are inappropriate. This is especially true for search algorithms based on deterministic search criteria. Even such quasi-random search algorithms as Simplex have progressive difficulties with an increase in the number of non-linear parameters. This reflects the simple fact that an increase in the number of non-linear parameters is usually accompanied by the emergence of additional local minima.

The random (Monte Carlo-based) nature of our main search procedure allows escape from local minima, while the adaptive nature of the algorithm provides a powerful tool for increasing the speed of conversion.

The search usually finds a "raw" approximation during the first 5–50 thousands of iterations. It is extremely important not to stop at this level, but to let the search algorithm crawl to the bottom of the RSMR well. In many cases, an approximation which seemed to be perfectly sensible after the first few thousands of iterations later produces such unrealistic features as strong negative absorption outside the main absorption band of the unphotolysed chromophore.

6.3. The strategy for applying SCHEMEFIT to selecting the 'best-fitting' kinetic scheme

The main strategic decision is the choice of models to be tested, their sequence, and the criteria of switching from one scheme to another. From a purely logical point of view, the best strategy should be to start with the most complicated model, which allows all transitions between all transient states. This corresponds to a **K**-matrix in which all elements except those on the main diagonal are non-zero, and then to let the fitting algorithm indicate the unneeded elements by driving the corresponding rate constants to zero [8,9]. Unfortunately, two facts make this theoretically most favorable approach non-practical. First, in really complex cases the corresponding programs sometimes fail to eliminate the unnecessary transition and even sometimes indicate a need to eliminate a valid transition (see also [9]). Second, an addition of one nonlinear parameter necessarily leads to an increase in the number of iterations (by approximately doubling the N_{fit} parameter in *SCHEMEFIT*), with subsequent drastic increase in the computational time.

Applying *SCHEMEFIT* to both synthetic and real data (see Section 7.1 and Section 7.2, respectively) led us to an alternative approach. Three values of RSMR from corresponding fits were used for decision-making:

1. RSMR values from global fitting of data separately at each temperature ($\mathrm{RSMR_{GF}}$);
2. The RSMR value from scheme-fitting to the simplest possible model: to the unidirectional unbranched cycle (e.g. O → A → B → C → D → O) ($\mathrm{RSMR_U}$);
3. The RSMR value from scheme-fitting to some cycle model which is expected to be more complex than the true one ($\mathrm{RSMR_O}$). For instance, to a model in which all back reactions are included (e.g. O → A ⇔ B ⇔ C ⇔ D ⇔ O, as compared to Eq. (22)).

The scheme in case #2 includes fewer transitions than the true scheme (see Eq. (22)); we shall call such schemes *underdetermined.* Alternatively, a scheme including more reactions than the true scheme (for instance, that of case #3) will be called *overdetermined.*

Unfortunately, application of statistical tests is much less straightforward in scheme-fitting analysis than in global fitting. The main difficulty is in estimating the residual degrees of freedom after fitting. In global fitting, the number of degrees of freedom is well-defined. Initially, the data contain $N_t \cdot N_\lambda$ independent points. A global fit with N_e exponentials at N_λ wavelengths/wavenumbers decreases the number of degrees of freedom by $\{N_\lambda \cdot (N_e + 1) + N_e\}$, since this is the number of parameters (and therefore data points) which unambiguously define a unique set of N_e exponential curves at N_λ wavelengths. Global fit is a phenomenological description which does not impose any restrictions on possible values of either exponentials or their amplitudes. However, this is not true for scheme-fitting. The problem is that all possible N_i intermediate models (starting from the simplest unidirectional un-

branching one and up to the most complex one) result in apparent kinetics with N_i exponentials and a constant level. Increasing the complexity of the model does not lead to a change in the number of terms in the series expansion of the apparent kinetics. However, unlike the phenomenological description with multi-exponentials, where the corresponding exponential amplitudes (eigen-vectors) could be fitted without any restrictions, any particular scheme-fitting model does impose restrictions on the corresponding eigen-vectors of true concentrations, and, therefore, on apparent kinetic amplitudes. The RSMR value from global fitting, $RSMR_{GF}$, gives the absolute minimum of RSMR for scheme-fitting. Any model, including the correct best-fitting one, would produce an RSMR value which is equal or greater than $RSMR_{GF}$, because the scheme-fitting minimization is performed as a search of a conditional minimum, while that of the GF is for an unconditional one. Thus, it is practically impossible to use the RSMR values to compare quantitatively two models with the same number of adjustable parameters but different topology [12]. Comparison of the RSMR value from global fitting, $RSMR_{GF}$, with $RSMR_O$ of the scheme, which is assumed to be overdetermined, serves as an indicator of whether the latter scheme is actually too complicated or is oversimplified. Based on experience with synthetic data, a model should be considered overdetermined when the ratio $RSMR_O/RSMR_{GF}$ is below 1.3–1.6. Higher values indicate that the model lacks complexity and additional transitions need to be included. At this step, any transition in the "forward" direction is always included together with the corresponding back reaction (e.g. both B → D and B ← D).

The next step is to simplify the kinetic scheme starting from the overdetermined model. The best way is to repeat the fits on all models differing from the overdetermined scheme, omitting only one particular allowed transition in each fit. In practice, back reactions with rate constants of at least 100 times slower than the rate constant in the forward direction ($k_{back}/k_{forward} < 10^{-2}$) are good candidates for elimination. Frequently, several transient balances (in an overdetermined scheme) have values of $k_{back}/k_{forward} < 10^{-2}$. From our experience, no more than one transition should be eliminated at a time in progressing from one tentative scheme to a simpler one, even if two or more balances qualify for $k_{back}/k_{forward} < 10^{-2}$. Note that if a fit to an overdetermined model produces several steps with $k_{back}/k_{forward} < 10^{-2}$, the lowest value of $k_{back}/k_{forward}$ does not always point to the insignificant transition. This rather points out that *at least one* insignificant transition is present in the tested scheme. Mathematically, this reflects the fact that in the multi-dimensional space of non-linear search parameters the RSMR hyper-surface is not only characterized by a variety of local minima, but is changed in a non-linear way upon changes in its dimensions. That is, RSMR minima shift, appear and disappear when some particular transition is removed from the fitted model. However, certain trends of the RSMR evolution from one scheme to another are really indicative. Stable or decreasing RSMR values are associated with elimination of an unneeded transition from an overdetermined scheme, while an increase in RSMR values indicates an attempt to eliminate a valid transition from the true scheme. Thus, the best-fitting scheme is found when any attempt to further simplify the tentative scheme leads to an obligatory increase in RSMR.

An interesting feature about overdetermined schemes is that when using them, *SCHEMEFIT* sometimes failed to converge during a reasonable time to an RSMR value corresponding to the exact scheme, but rather stopped at values of RSMR approx. 30% higher. Furthermore, much lower values of RSMR were produced within approximately the same number of iterations when the tentative scheme was simplified. Insufficient number of iterations used (i.e. N_{fit} was too low), loss of accuracy due to accumulation of a roundoff error, or insufficient sensitivity of data to small model variations (e.g. due to a too narrow range of temperature for which the data was measured), are the most probable reasons for this seemingly unexpected behavior. Alternatively, this might indicate some limitations of the approach (e.g. insufficient accuracy of search in the space of more than 14 non-linear parameters), or might be due to changes in the RSMR hyper-surface induced by dimensional changes in the search space.

[12] E.g. two schemes: (i) O → A ⇔ B ⇔ C ⇔ D → O and A ⇔ C, and (ii) O → A ⇔ B ⇔ C ⇔ D → O and B ⇔ D.

7. Application of *SCHEMEFIT*

7.1. Analysis of synthetic data

To test the performance of *SCHEMEFIT*, 3D arrays of synthetic data were generated with variable amounts of white noise for the same model as in Section 5 (Eq. (22)), using the same spectra of Fig. 1. The 2D data shown in Fig. 3 (called "data at 20°C" below) were included in this 3D array together with simulated data at 10°C and 30°C. Temperature dependencies for particular rate constants were assumed to be in accordance with Eyring's law (Eq. (9)), with $\Delta H^{\#}$ in the range from 10 to 60 kJ M^{-1}, and $\Delta S^{\#}$ in the range from -0.2 to -0.03 kJ $M^{-1}°C^{-1}$, and corresponding $\Delta G^{\#}$ values from 56 to 67 kJM^{-1}. The excitation efficiency, $\varphi(T)$, was assumed to be 0.23, 0.30 and 0.20 at 10°, 20°, and 30°C, to further complicate the task for the scheme-fitting program. Only the 3D arrays with $S/N \geq 250$ were subjected to scheme-fitting analysis.

A scheme with all back reactions but without branching (for both $S/N = 320$ and $S/N = 640$) already produced RSMR values approximately 30% above that of the global fitting. In the strict sense, this is not a sufficient argument to reject the possibility of branching reactions, so additional branching reactions were added to the scheme already including all back reactions. This failed to improve the RSMR significantly, so the scheme without branching but with all back reactions was considered to be overdetermined. In this scheme the highest value obtained for $k_{forward}/k_{back}$ was $k_{D \to O}/k_{O \to D} \cong 50$, correctly indicating the O → D transition, which was not present in the assumed true scheme used to generate the synthetic data. Eliminating this transition from the kinetic scheme indeed produced a more significant reduction in RSMR than dropping any other back reaction, thus verifying that this transition is not needed. The B → A transition was eliminated on the next step in a similar way, and a scheme O → A → B ⇔ C ⇔ D → O, equivalent to the true one, was obtained. The RSMR values at this stage were some 10% above the noise level (and therefore still above the $RSMR_{GF}$). Attempts to further simplify the tentative scheme led to increases in RSMR, indicating that all transitions in the scheme O → A → B ⇔ C ⇔ D → O are significant. Fig. 7 presents the spectra calculated by *SCHEMEFIT* from data with $S/N \geq 320$. Note, that this result was obtained on the same set of data ($S/N = 320$), for which SVD failed even to estimate correctly the number of intermediates involved.

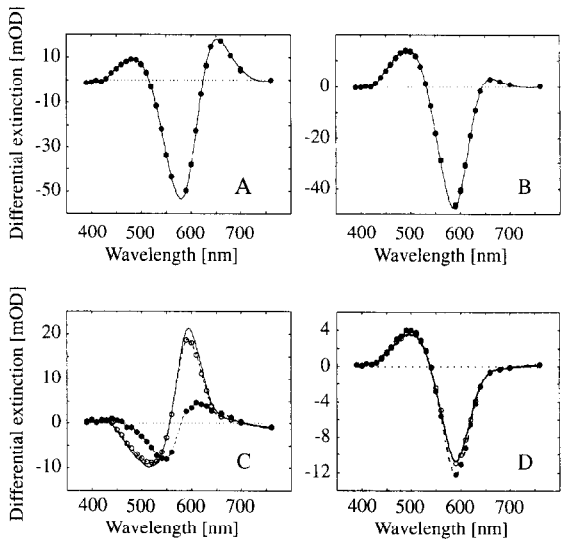

Fig. 7. Differential spectra of intermediates extracted by the *SCHEMEFIT* program, which fitted the synthetic data with $S/N \geq 320$ (see Fig. 3) directly to the set of coupled differential equations. The solid line is for the case of noiseless data; it is indistinguishable from the intermediates' spectra in Fig. 1. The dashed line with open circles is for $S/N = 640$; the dashed-dotted line with filled circles is for $S/N = 320$. The differences in spectra calculated from data with different S/N ratios could be seen only for state C and to some extend for state D.

In the case of noiseless data, the spectra produced by *SCHEMEFIT* were practically indistinguishable from the spectra used for simulations. The average difference was 0.03 mOD for the spectra with amplitudes of at least 10 mOD (see Fig. 1 and Fig. 7).

Comparison of spectra used for simulations (Fig. 1) with amplitude spectra from GF (Fig. 4), basis spectra from SVD (Fig. 5) and calculated differential spectra by *SCHEMEFIT* (Fig. 7), illustrates the power of the scheme-fitting program.

7.2. Analysis of the halorhodopsin photocycle

This section illustrates the use of *SCHEMEFIT* on real data. Preliminary results of this study were reported earlier [18,61–63]. Full details are to be published elsewhere (A.K. Dioumaev and D. Oester-

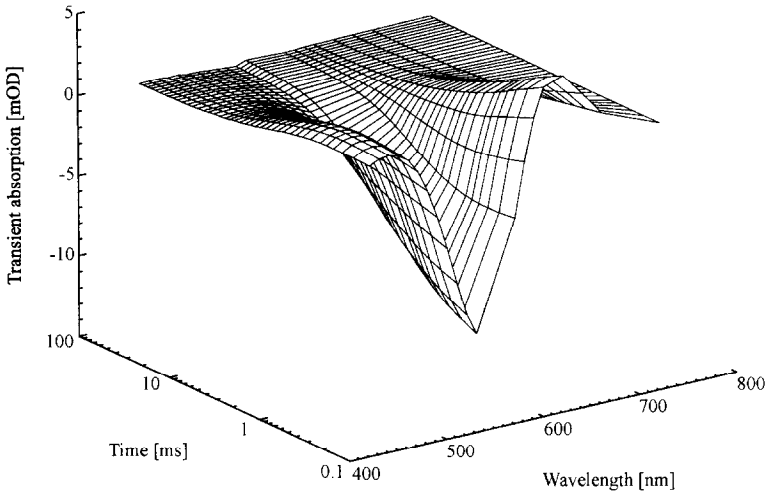

Fig. 8. Transient absorption changes associated with the photocycle of halorhodopsin at 20°C at pH 7.0 in the presence of 1 M NaCl.

helt, in preparation). Fig. 8 presents a typical time-course of absorption changes associated with the halorhodopsin photocycle at high salt (NaCl) concentrations. Global fitting by *FITEXP* indicates the presence of four transient intermediates at each of the 4 temperatures (from 8°C to 30°C) for which the data were measured. Additional analysis of the distribution of residuals in each 2D array confirmed 4 intermediates: the addition of the fourth exponent in the GF analysis removed any systematic deviations, and the residual array became random. The apparent rate constants, $\mathbf{k}_{GT}$, displayed smooth temperature dependence, though not exactly Arrhenius. The corresponding amplitude spectra were well defined, but displayed distinct systematic variations with temperature. Both of these two features clearly indicate that the kinetic scheme of the halorhodopsin photocycle is more complex than a simple sequential unidirectional one.

Using the above outlined strategy, a four-intermediate cycle (intermediates B, C, D, E [13]) was fitted to experimental data with *SCHEMEFIT*. All possible schemes with one state in a *cul-de-sac* (the way the hR_{410} side-product might be expected to appear [64]) were tried and rejected. This is in accordance with the earlier evidence that hR_{410} appears only after prolonged continuous illumination [64]. Fitting a 3D data array to the simplest linear unidirectional photocycle, $hR \rightarrow hR_{600} \rightarrow B \rightarrow C \rightarrow D \rightarrow E \rightarrow hR$, produced an $RSMR_U$ value that was 36% higher than for the $hR \rightarrow hR_{600} \rightarrow B \Leftrightarrow C \Leftrightarrow D \Leftrightarrow E \Leftrightarrow hR$ model. This difference clearly indicates that some of the four back reactions are significant. Adding branching reactions failed to improve the RSMR significantly. Systematic elimination of back reactions indicated that the only really significant one (at 1 M NaCl concentration) is the $D \rightarrow C$ transition. As a result, the following scheme was considered to be best-fitting

$$hR \rightarrow hR_{600} \rightarrow B \rightarrow C \Leftrightarrow D \rightarrow E \rightarrow hR \qquad (26)$$

This 5-transition model was found to be inferior only to a 9-transition scheme, in which besides all back reactions, a branching pathway between the B and E states was included. However, given the similarity of spectra for both schemes, the much simpler scheme (Eq. (26)) can be considered to be the best-fitting scheme. Calculated differential spectra are presented in Fig. 9.

These differential spectra (Fig. 9) revealed that the 'B' and 'D' states are bathochromic, 'C' state is

[13] The use of blind letters is to further re-iterate, that no *a priori* assumptions were made on the intermediates spectra. The letter A is reserved for a fast-decaying bathochromic state, hR_{600}, which is present only during the first several microseconds in the cycle [58].

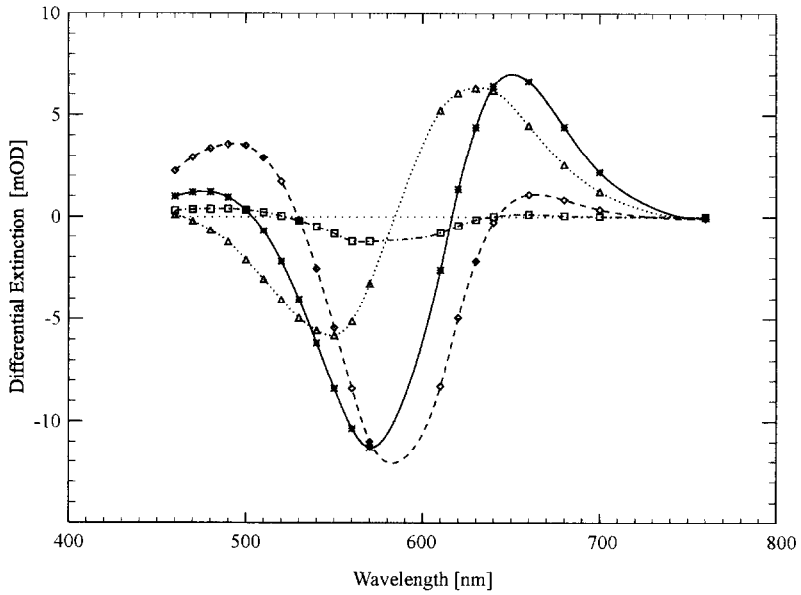

Fig. 9. Differential spectra for the best-fitting model hR → A_{600} → B → C ⇔ D → E → hR, extracted by *SCHEMEFIT* from a multi-wavelength, multi-temperature data; the 20°C component of this data set is presented in Fig. 8. Intermediate B, solid line and asterisks; C, dashed line and diamonds; D, dotted line and triangles; E, dash-dotted and squares.

hypsochromic, and the state 'E' is characterized by practically the same spectrum as the initial (parent) state of non-photolysed pigment, but with a lower extinction coefficient. The corresponding photointermediate concentrations are presented in Fig. 10. Based on the published values of the quantum yield

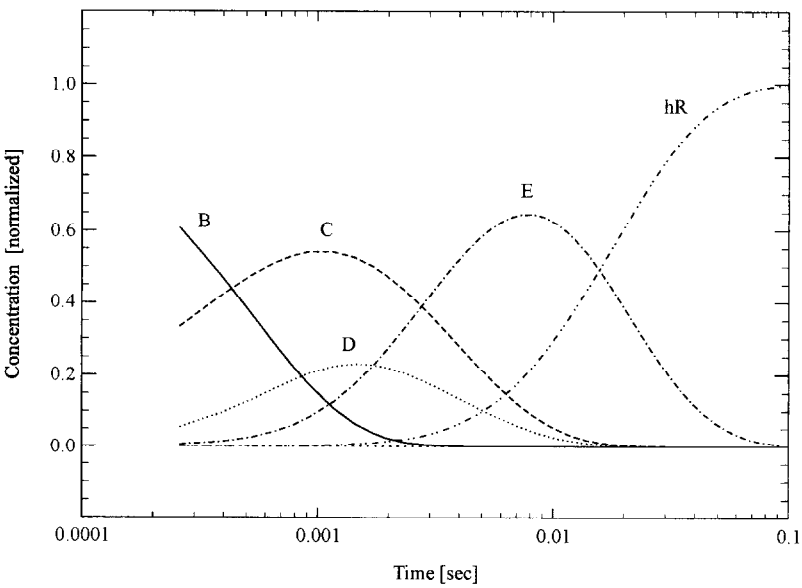

Fig. 10. True concentration kinetics of the four intermediates in the halorhodopsin photocycle for the best-fitting scheme, extracted by *SCHEMEFIT*. Intermediate B, solid line; C, dashed; D, dotted; E, dash-dotted; hR recovery, dash-double-dotted.

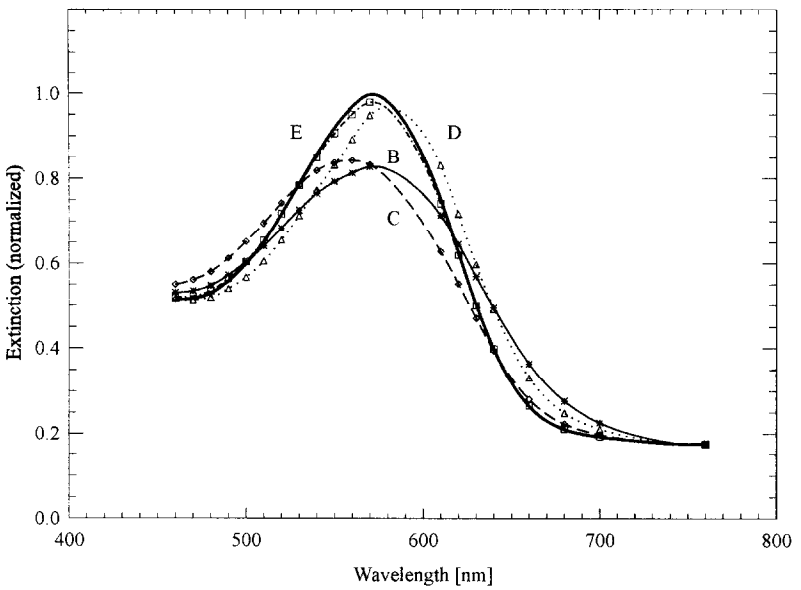

Fig. 11. Absolute spectra of halorhodopsin photocycle intermediates, recalculated from differential spectra in Fig. 9. Intermediate B, solid line and asterisks; C, dashed and diamonds; D, dotted and triangles; E, dash-dotted and squares. The thick line is the halorhodopsin absorption spectrum.

of the halorhodopsin photocycle [64], an upper limit for excitation efficiency, φ, was estimated at $\leq 20\%$. Attempts to reconstruct absolute spectra, assuming values for $\varphi \leq 8\%$, resulted in secondary maxima in spectra of states 'B' and 'C'. Absolute spectra for $\varphi = 0.15$ are shown in Fig. 11.

Initial heterogeneity of the halorhodopsin chromophore in the ground state (hR_{13-cis} and $hR_{13-trans}$) which might give rise to a mixture of intermediates from two parallel photocycles in the studied time range (as proposed in Ref. [19]) was not considered here, and will be treated elsewhere (A.K. Dioumaev and D. Oesterhelt, in preparation).

8. Conclusions

Using synthetic data we have demonstrated that widely used methods for mathematical analysis of 2D spectral-kinetic data fail to extract true spectra of the transient states and true kinetics of their concentrations. Instead, global fitting, singular value decomposition, principal component analysis and factor analysis produce only phenomenological description, which does not allow a correlation of experimentally measured data with the underlying molecular mechanism.

All these shortcomings can be overcome by including additional data at different temperatures to form a 3D experimental array to be fitted simultaneously to systems of differential equations describing tentative kinetic schemes. The scheme-fitting analysis permits the best-fitting scheme to be found, and the calculation of all its intrinsic parameters. This is illustrated on synthetic data with a custom-built program, *SCHEMEFIT*. The ability of *SCHEMEFIT* to recalculate true spectra and intrinsic kinetics, as well as to evaluate the paths of the transient states' interconversions, is in evident contrast with GF and SVD analyses, both of which failed to perform this task. *SCHEMEFIT* performance on real data is included as an additional illustration of the prospective power of the scheme-fitting approach to studies of natural photochromes.

The advantage of scheme-fitting analysis is in extracting intrinsic molecular parameters. This information is extremely important for evaluating the molecular mechanism of function, which otherwise remains hidden behind the apparent multi-component kinetics of complex systems. We believe that the 3D

scheme-fitting analysis will become a widely used 'instrument' in the years to come for studying different complex chemical reactions, which include a number of transient states with complex paths of their interconversions.

9. Notes added in proof

While this paper was under consideration we were able to obtain an independent confirmation for one of the most controversial results presented above. This concerns our conclusion (in Section 7.2) on the existence in the main path of halorhodopsin photocycle of a second bathochromic intermediate, B, with a lifetime of 500 μs (at 20°C) following the primary bathochromic state, hK_{600}, but prior to hypsochromic intermediate C (see Figs. 9 and 10). No such intermediate was ever included in the previous schemes of the halorhodopsin photocycle [19,58,64,65]. Recent time-resolved FTIR measurements with nanosecond time-resolution (Dioumaev & Braiman, in preparation) revealed existence of a transient state with a rise time of ~ 300 ns and decay time of ~ 400 μs (at 20°C). (Experiments were performed at pH 7.3 in the presence of 2 M NaCl on a sample prepared from the same strain of halorhodopsin as used in this paper). The pattern and the magnitude of the transient absorption changes in both ethylenic and hydrogen out-of-plane (HOOP) regions unambiguously signal that this intermediate is the second K-like state, hK_L (or 'late K'). It is directly formed from the primary bathointermediate, hK_{600} (or 'early K'), described earlier [58]. The hK_L intermediate detected in the IR belongs to the main photocycle path originating from the *all-trans* chromophore, and it decays into the well-known L-like state, hL [19,58,64,65] (alias our intermediate C, see Fig. 9). Spectral and kinetic properties of the hK_L intermediate are fully consistent with the properties of the intermediate B proposed in this paper, thus independently confirming both the origin and the placement of B in the kinetic scheme (Eq. (26), Figs. 9 and 10).

Acknowledgements

This work was in part supported by the Alexander von Humboldt Foundation and the Fogarty International Center to the author, who was an Alexander von Humboldt Research Fellow in 1993–1994, and a Fogarty International Fellow in 1995–1996. Other funding included grants from the Russian Academy of Science, while the author was an employee of the General Physics Institute of the Russian Academy of Sciences, Moscow, Russia. The author would like to express his gratitude to Prof. Dieter Oesterhelt for hospitality, support and encouragement, and to Prof. M.S. Braiman for many critical comments on the manuscript. Many helpful discussions with Prof. J.F. Nagle, Drs. R.H. Lozier, N.V. Tkachenko and V.I Chukharev are gratefully acknowledged. Thanks are also due to the staff of the computer centers in MPIB, Martinsried and UVa, Charlottesville.

References

[1] J.F. Nagle, L.A. Parodi, R.H. Lozier, Biophys. J., 38 (1982) 161.
[2] A. Xie; J.F. Nagle, R.H. Lozier, Biophys. J., 51 (1987) 627.
[3] R. Maurer, J. Vogel, S. Schneider, Photochem. Photobiol., 46 (1987) 247 and 255.
[4] J. Hofrichter, E.R. Henry, R.H. Lozier, Biophys. J., 56 (1989) 693.
[5] J.B. Ames, R.A. Mathies, Biochemistry, 29 (1990) 7181.
[6] K. Gerwert, G. Souvigner, B Hess, Proc. Natl. Acad. Sci. USA, 87 (1990) 9774.
[7] Gy. Váró, J.K. Lanyi, Biophys. J., 59 (1991) 313.
[8] J.F. Nagle, Biophys. J., 59 (1991) 476.
[9] J.F. Nagle, Photochem. Photobiol., 54 (1991) 897.
[10] K.-H. Muller, H.J. Butt, E. Bamberg, K. Fendler, B. Hess, F. Siebert, M. Engelhard, Eur. Biophys. J., 19 (1991) 241.
[11] W.G. Chen, M.S. Braiman, Photochem. Photobiol., 54 (1991) 905.
[12] A.Yu. Sharonov, N.V. Tkachenko, V.V. Savransky, A.K. Dioumaev, Photochem. Photobiol., 54 (1991) 889.
[13] R.H Lozier, A. Xie, J. Hofrichter, G.M. Clore, Proc. Natl. Acad. Sci. USA, 89 (1992) 3610.
[14] B. Heßling, G. Souvigner, K. Gerwert, Biophys. J., 65 (1993) 1929.
[15] L. Zimányi, J.K. Lanyi, Biophys. J., 64 (1993) 240.
[16] Y. Cao, Gy. Váró, A.L. Klinger, D.M. Czajkowsky, M.S. Braiman, R. Needleman, J.K. Lanyi, Biochemistry, 32 (1993) 1981.
[17] J.F. Nagle, L. Zimanyi, J.K. Lanyi, Biophys. J., 68 (1995) 1490.
[18] A.K. Dioumaev, D. Oesterhelt, Abstracts of the 6th Int. Conf. on Retinal Proteins, Lieden, The Netherlands, 1994.
[19] Gy. Váró; L. Zimanyi, X. Fan, L. Sun, R. Needleman, J.K. Lanyi, Biophys. J., 68 (1995) 2062.

[20] Gy. Váró, L.S. Brown, J. Sasaki, H. Kandori, A. Maeda, R. Needleman, J.K. Lanyi, Biochemistry, 34 (1995) 14490.
[21] S.J. Hug, J.W. Lewis, C.M. Einterz, T.E. Thorgeirsson, D.S. Kliger, Biochemistry, 29 (1990) 1475.
[22] A.L. Klinger, M.S. Braiman, Biophys. J., 63 (1992) 1244.
[23] T.E. Thorgeirsson, J.W. Lewis, S.E. Wallace-Williams, D.S. Kliger, Photochem. Photobiol., 56 (1992) 1135.
[24] K.E. Georgiadis, N.-I. Jhon, Ó. Einarsdóttir, Biochemistry, 33 (1994) 9245.
[25] Ó. Einarsdóttir, K.E. Georgiadis, A. Sucheta, Biochemistry, 34 (1995) 496.
[26] C.-F. Zhang, D.L. Farrens, S.C. Björling, P.-S. Song, D.S. Kliger, J. Am. Chem. Soc, 114 (1992) 4569.
[27] J. Horfricher, E.R. Henry, J.H. Sommer, R. Deutch, M. Ikeda-Saito, T. Yonetani, W.A. Eaton, Biochemistry.,24 (1985) 2667.
[28] W.D. Hoff, I.H.M. van Stokkum, H.J. van Ramesdonk, M.E. van Brederode, A.M. Brouwer, J.C. Fitch, T.E. Meyer, R. van Grondelle, K.J. Hellingwerf, Biophys. J., 67 (1994) 1691.
[29] K. Ng, E. Getzoff, K. Moffat, Biochemistry, 34 (1994) 879.
[30] G.H. Golub, V. Pereyra, SIAM (Soc. Ind. Appl. Math.) J. Numerical Analysis, 10 (1973) 413.
[31] G.H. Golub, R.J. Leveque, Proc. Army Numerical Analysis and Computing Conference, ARO Report, 79-3 (1979) 1.
[32] J.M. Beechem, Meth. Enzymol., 210 (1992) 37.
[33] G.H. Golub, W.J. Kahan, J. SIAM (Soc. Ind. Appl. Math.) Numer. Anal. Ser. B, 2 (1965) 205.
[34] G.H. Golub, C. Reinsch, Numer. Math., 14 (1970) 403.
[35] R.I. Shrager, SIAM (Soc. Ind. Appl. Math) J. Alg. Disc. Meth., 5 (1984) 351.
[36] E.R. Henry, J. Hofrichter, Meth. Enzymol., 210 (1992) 129.
[37] S.D. Frans, J.M. Harris, Anal. Chem., 57 (1985) 1718.
[38] R.I. Shrager, Chemometrics and Intelligent Laboratory Systems, 1 (1986) 59.
[39] N.V. Tkachenko, Ph.D. thesis, General Physics Institute of the Academy of Sciences of the USSR, Moscow, 1989.
[40] W.H. Press, B.P. Flannery, S.A. Teukolsky, W.T. Vetterling, Numerical recipes in C. The art of scientific computing, Cambridge University Press, Cambridge, 1988.
[41] J.A. Heymann, W.A. Havelka, D. Oesterhelt, Molecular Microbiology, 7 (1993) 623.
[42] R. Uhl, B. Meyer, H. Desel, J. Biochem. Biophys. Meth., 10 (1985) 35.
[43] L. Onsager, Phys. Rev., 37 (1931) 405.
[44] A.K. Dioumaev, V.V. Savransky, N.V. Tkachenko, V.I. Chukharev, J. Photochem. Photobiol. B., 3 (1989) 385.
[45] D.L. Massart, B.G.M. Vandeginste, S.N. Deming, Y. Michotte, L. Kaufman, Chemometrics: a Textbook, Elsevier, Amsterdam, 1988.
[46] E.R. Malinowski, Factor Analysis in Chemistry, 2nd edn., John Wiley and Sons, Ltd., New York, 1991.
[47] S. Glasstone, K.J. Laidler, H. Eyring, The Theory of Rate Processes: The Kinetics of Chemical Reactions, Viscosity, Diffusion and Electrochemical Phenomena, McGraw-Hill Book Company, New York and London, 1941.
[48] L. Kaufman, Bit., 15 (1975) 49.
[49] S.D. Frans, J.M. Harris, Anal. Chem., 56 (1984) 466.
[50] K.-H. Muller, T. Plesser, Eur. Biophys. J., 19 (1991) 231.
[51] P.R. Bevington, Data Reduction and Error Analysis for The Physical Sciences, McGraw-Hill Book Company, New York, 1969, Chapt. 10.
[52] P.R. Bevington, D.K. Robinson, Data Reduction and Error Analysis for the Physical Sciences, 2nd edn., McGraw-Hill Book Company, New York, 1992, Chapt. 11.
[53] E.R. Malinowski, Anal. Chem., 49 (1977) 606.
[54] E.R. Malinowski, Anal. Chem. 49 (1977) 612.
[55] R. Kramer, Chemometrics Toolbox User's Guide, The Math Works Inc., 1992.+
[56] R.I. Shrager, R.W. Hendler, Anal. Chem., 54 (1982), 1147.
[57] Gy. Váró, J.K. Lanyi, Biochemistry, 30 (1991) 5008.
[58] J. Tittor, D. Oesterhelt, R. Maurer, H. Desel, R. Uhl, Biophys. J., 52 (1987) 999.
[59] L. Pronzato, E. Walter, A. Venot, J.-F. Lebruchec, Math. and Comput. Simulation, 26 (1984) 412.
[60] MINUIT - Function Minimization and Error Analysis, (Reference Manual, Version 92.1.), CERN Program Library Long Writeup D506, CERN, Geneva, 1992.
[61] A.K. Dioumaev, Abstracts of the 22nd FEBS Meeting, #89, Stockholm, Sweden, 1993, p.187.
[62] A.K. Dioumaev, Abstracts of the Int. Symposium on Biological Physics: Dynamics and Function of Biomembranes, Szeged, Hungary, 1993.
[63] A.K. Dioumaev, J. Tittor, D. Oesterhelt, Abstracts of the 11th Int. Biophys. Cong., # E2.15, Budapest, Hungary, 1993, p. 196.
[64] P. Hegemann, D. Oesterhelt, M. Steiner, EMBO J, 4 (1985) 2347.
[65] D. Oesterhelt, P. Hegemann, J. Tittor, EMBO J., 4 (1985) 2351.